

**Confined Trapped-Alpha Behaviour  
in TFTR Deuterium-Tritium Plasmas**

S. S. Medley, R. V. Budny, H. H. Duong<sup>1</sup>, R. K. Fisher<sup>1</sup>, M. P. Petrov<sup>2</sup>,  
N. N. Gorelenkov<sup>3</sup>, M. H. Redi, A. L. Roquemore, and R. B. White

*Princeton Plasma Physics Laboratory, P. O. Box 451, Princeton, New Jersey 08543 USA*

*<sup>1</sup>General Atomics, San Diego, California 92186 USA, <sup>2</sup>A. F. Ioffe Physical-Technical Institute,  
St. Petersburg, 194021 Russia, <sup>3</sup>TRINITI, Troitsk 142092 Russia*

**Abstract**

Confined trapped-alpha energy spectra and differential radial density profiles in TFTR D-T plasmas are obtained with the Pellet Charge-eXchange (PCX) diagnostic which measures high energy ( $E_\alpha = 0.5 - 3.5$  MeV), trapped alphas ( $v_{||}/v = -0.048$ ) at a single time slice ( $\Delta t \sim 1$  ms) with a spatial resolution of  $\Delta r \sim 5$  cm. Tritons produced in D-D plasmas and RF-driven ion tails (H,  $^3\text{He}$  or T) were also observed and energetic tritium ion tail measurements will be discussed.

PCX alpha and triton energy spectra extending up to their birth energies were measured in the core of MHD-quiet discharges where the expected classical slowing down and pitch angle scattering effects are not complicated by stochastic ripple diffusion and sawtooth activity. Both the shape of the measured alpha and triton energy distributions and their density ratios are in good agreement with TRANSP predictions, indicating that the PCX measurements are consistent with classical thermalization of the fusion-generated alphas and tritons. From calculations, these results set an upper limit on possible anomalous radial diffusion for trapped alphas of  $D_\alpha \leq 0.01 \text{ m}^2\text{s}^{-1}$ . Outside the core, where the trapped alphas are influenced by stochastic ripple diffusion effects, the PCX measurements are consistent with the functional dependence of the Goldston-White-Boozer stochastic ripple threshold on the alpha energy and the q-profile.

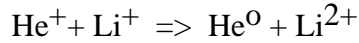
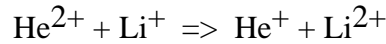
In the presence of strong sawtooth activity, the PCX diagnostic observes significant redistribution of the alpha signal radial profile wherein alphas are depleted in the core and redistributed to well outside the  $q = 1$  radius, but apparently not beyond the energy-dependent stochastic ripple loss boundary. The helical electric field produced during the sawtooth crash plays an essential role in modeling the sawtooth redistribution data. In sawtooth-free discharge scenarios with reversed shear operation, the PCX diagnostic also observes radial profiles of the alpha signal that are significantly broader than those for supershots. ORBIT modeling of reversed shear and monotonic shear discharges are in agreement with the q-dependent alpha profiles observed. Redistribution of trapped alpha particles in the presence of core localized TAE activity was

observed and modeling of the PCX measurements based on a synergism involving the  $\alpha$ -TAE resonance and the effect of stochastic ripple diffusion is in progress.

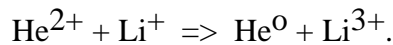
## 1.0 INTRODUCTION

The deuterium-tritium operation of TFTR [1] has provided an opportunity to extend previous observations of fast ion behaviour in tokamaks [2] to alpha particles generated in D-T plasmas [3]. Several diagnostics designed to measure confined alphas in large tokamaks were used in the TFTR experiments; namely, charge exchange recombination spectroscopy [4] microwave scattering [5], and energetic neutral particle analysis with the use of low-Z impurity pellets [6,7]. The last method, which we call Pellet Charge eXchange (PCX), was operated routinely on TFTR during D-T experiments [8]. PCX diagnostic results have been reported on measurements of RF-driven energetic H,  $^3\text{He}$  and T minority ion tails [9-11], the energy distribution fast confined alpha particles [12,13], and the influence of magnetic field ripple and sawtooth oscillations on the behaviour of the alpha energy spectra and radial profiles of the alpha signal [14-17].

In the PCX diagnostic on TFTR, low-Z impurity pellets are injected along a midplane major radius. Upon entering the plasma, the pellet forms a toroidally elongated ablation cloud, as illustrated in Fig. 1. Using lithium pellets as an example, a small fraction of the alphas incident on the ablation cloud is neutralized either by sequential single electron capture,



or by double electron capture



If the line integral target density for particles traversing the cloud is sufficiently large, then the fraction of particles emerging from the cloud as neutrals approaches the equilibrium fraction,  $F_0^\infty(E)$ , which is independent of the linear density of the cloud. Pitch angle scattering and energy loss are not important at the pellet ablation cloud densities expected in TFTR [18]. By measuring the energy distribution,  $dn_0/dE$ , of the resultant helium neutrals escaping from the plasma, the energy distribution of the incident alpha particles,  $dn_\alpha/dE$ , can be determined using

$$dn_\alpha/dE \propto K(E) dn_0/dE \quad (1)$$

where

$$K(E) = \left\{ F_0^\infty(E) v_\alpha \frac{\Omega}{4\pi} \eta(E) \Delta E \right\}^{-1} \quad (2)$$

and

$$\begin{aligned}
 F_0^\infty(E) &= \text{neutral equilibrium fraction,} \\
 v_\alpha &= \text{ion velocity associated with energy } E, \\
 \frac{\Omega}{4\pi} &= \text{solid angle of the analyzer,} \\
 \eta(E) &= \text{calibrated analyzer detection efficiency, and} \\
 \Delta E &= \text{energy resolution of the analyzer.}
 \end{aligned}$$

The neutral equilibrium fractions,  $F_0^\infty(E)$ , used for alphas and tritons are obtained from modeling calculations [12,18]. The neutral particle analyzer (NPA) detection efficiency,  $\eta(E)$ , was calibrated [19] for alphas using megavolt helium ion beams generated by a cyclotron accelerator and was derived for tritons using hydrogen ions. Note that  $K(E)$  must be evaluated for the individual NPA channels.

The escaping helium neutrals are mass and energy analyzed using a high energy (0.3 - 3.7 MeV for  $^4\text{He}$ ) neutral particle analyzer [19]. The neutral particle analyzer views the cloud surrounding the radially injected pellet from behind at a toroidal angle of  $2.75^\circ$  to the trajectory of the pellet. As a result, only near perpendicular energetic ions with velocities close to  $v_{\parallel}/v = -0.048$  are detected by the PCX diagnostic. The radial position of the pellet as a function of time is measured using a linear photo diode array situated on the top of the vacuum vessel. By combining this measurement with the time dependence of the PCX signal, radially resolved fast ion energy spectra and radial profiles of the alpha signal can be derived with a radial resolution of  $\sim 5$  cm.

It should be noted that the radial profiles of the alpha signal measured by the PCX diagnostic are actually "differential density profiles"; that is,  $dn_\alpha/(dE d\Omega)$  ( $\text{m}^{-3}\text{MeV}^{-1}\text{ster}^{-1}$ ) where  $dE$  and  $d\Omega$  are the instrumental energy resolution and acceptance solid angle, respectively. The differential density profiles are relative measurements, since the PCX diagnostic is not absolutely calibrated. While the instrumental response of the NPA was absolutely calibrated, the absolute efficiency for neutralization of the measured ions by the pellet ablation cloud is uncertain due to uncertainties in the spatial distribution of ionization states in the cloud. It has been shown that provided the line integral cloud density is sufficiently high so that the charge changing reactions are independent of the density and attain an equilibrium fraction, as expected in the TFTR applications, the details of the pellet ablation cloud have little effect on the measured energy distribution but do have a strong effect on the absolute alpha density measurements [18].

The experimental data are compared with modeling results obtained using TRANSP [20]. TRANSP is a  $1\frac{1}{2}$ -dimensional transport code (calculations of magnetic equilibrium are two-dimensional) that uses measured plasma parameters with minimal additional assumptions to model

plasma discharges and includes modeling of stochastic ripple diffusion of alphas [21]. In TRANSP, the electron temperature is obtained from electron cyclotron emission [22], electron density from infrared interferometry [23], and ion temperature and toroidal rotational velocity from charge exchange spectroscopy [24]. Of special importance for interpretation of the PCX data is the  $q$ -profile, which is obtained from motional Stark effect measurements [25]. The recycling of wall neutrals and  $Z_{\text{eff}}$  (assumed radially flat) are inferred from spectroscopic measurement of the deuterium alpha emission and visible Bremsstrahlung data [26]. Monte Carlo techniques are used to follow energetic alpha and triton ion orbits as they thermalize and is then used to deduce the full energy and radial distribution of each species. The code assumes the alpha particles and tritons are well confined and slow down classically and includes the effects of Coulomb pitch angle scattering and velocity diffusion, but does not account for broadening of fusion-generated particles about their birth energy due to the kinetic energy of the reacting ions [27].

TRANSP provides a good calculation of the alpha and triton distributions integrated over all pitch angles. TRANSP divides the pitch angle range of  $\pm 1$  into 50 equally spaced bins, giving a pitch angle resolution of 0.04. The instrumental resolution is approximately  $\pm 10^{-3}$  around the mean pitch angle value of  $v_{\parallel}/v = -0.048$ . In order to reduce the Monte-Carlo statistical noise on the computed alpha spectra to an acceptable level, the pitch angle window in the TRANSP output cannot be constrained to less than  $-0.2 < v_{\parallel}/v < 0.2$ , which is large compared to the narrow instrumental window. Fortunately, the alpha distribution has a weak dependence on pitch angle in this range and does not exhibit any fine grain structure. The radial averaging used in TRANSP is  $0.05r/a$  for thermal particles and  $0.1r/a$  for fast ions. For the discharges used in this paper,  $a = 80$  cm. Thus the radial averaging in TRANSP for energetic alphas and tritons is  $\sim 8$  cm compared with the instrumental value of  $\sim 5$  cm

For proper simulation of the PCX measurements, however, the pitch angle should be constrained to account for only the deeply trapped particles. Although the TRANSP code is a powerful tool for analyzing experimental results, the Monte Carlo basis makes the code computationally intensive for modeling the PCX measurements. For this reason, a Fokker-Planck Post-TRANSP (FPPT) processor code [28] was developed which is based on a numerical solution of the drift-averaged Fokker-Planck equation using the method of integration over the particle characteristics [29]. FPPT uses the radial and energy profiles of the pitch angle integrated alpha source from TRANSP to calculate alpha distributions for experimental conditions specific to the PCX measurements. The FPPT code assumes that for the processes with characteristic times greater than the  $\alpha$ -particle bounce period, which is  $\tau_b \sim 10^{-6} - 10^{-5}$  s in TFTR, the distribution function of  $\alpha$ -particles can be represented as a function of particle constants of motion versus time:

$$f_{\alpha} = f_{\alpha}(v, \mu, P_{\phi}) \quad (3)$$

where

$$\mu = \frac{m(1 - v_{||}/v)^2}{2B}, \quad P_{\phi} = \frac{e_{\alpha}\psi}{2\pi m_{\alpha}c} - \frac{v_{||}RB_{\phi}}{B}; \quad (4)$$

where  $\psi$  is the poloidal magnetic flux. The corresponding drift orbit averaged Fokker-Planck equation for the  $\alpha$ -particle distribution function is [30]

$$\frac{\partial f_{\alpha}}{\partial t} = \langle St(f_{\alpha}) \rangle + \langle S_{\alpha} \rangle - \frac{f_{\alpha}}{\tau_{\delta}}, \quad (5)$$

where  $\langle \dots \rangle$  denotes the time averaging over the  $\alpha$ -particle drift orbit, and

$$S_{\alpha} = S_{TR}(r,t) \frac{\exp(-(v-v_{\alpha 0})^2/v_T^2)}{\sqrt{\pi v_{\alpha 0}^2 v_T}} \quad (6)$$

is the  $\alpha$ -particle source with  $S_{TR}(r,t)$  taken from the TRANSP code, and  $v_T$  is the Doppler broadening. Equation 6 assumes Maxwellian distributions for the interacting species and gives a good approximation for beam-target interactions. The collisional integral given by

$$St(f_{\alpha}) = \frac{1}{v^2 \tau_S} \frac{\partial(v^3 + v_*^3)f_{\alpha}}{\partial v} + \frac{1}{\tau_S} \left( P_{\phi} - \frac{e_{\alpha}\psi}{2\pi m_{\alpha}c} \right) \left( 1 + \frac{v_*^3}{v^3} \right) \frac{\partial f_{\alpha}}{\partial P_{\phi}}, \quad (7)$$

where  $\tau_S$  is the slowing down time, describes only the slowing down of alphas and does not include pitch angle scattering and velocity diffusion [30]. The last term in Eq. 5 is introduced to account for the stochastic ripple losses, with  $\tau_{\delta}$  being the approximate confinement time associated with this loss process. The term  $\tau_{\delta}$  was derived by Yushmanov [31] and takes the form

$$\tau_{\delta} = \frac{(a-r)^2}{D_{\perp}} \quad (8)$$

where

$$D_{\perp} = \frac{(\Delta r)^2}{\tau_b} \text{ is the diffusion coefficient,} \quad (9)$$

$$(\Delta r)^2 = \frac{\pi \rho^2 q^3 N \delta^2(r_b, \theta_b)}{2 \epsilon^3 \sin \theta_b [1 + \exp(6.9 - 5.5\alpha)]} \quad (10)$$

and

$$\alpha = \left( \frac{8\pi N^3 q^5 R^3}{\omega_c^2 r^5} \right)^{1/2} v \delta(r_b, \theta_b) \frac{\theta_b S + \cot \theta_b}{\sqrt{\sin \theta_b}}. \quad (11)$$

In Eq. 9,  $\Delta r$  is the radial step size during one bounce period and  $r_b$ ,  $\theta_b$  are the radial and poloidal coordinates of the banana tip, respectively.

## 2.0 PCX MEASUREMENTS IN MHD-QUIESCENT PLASMAS

The alpha particle distributions measured by the PCX diagnostic can be influenced by the effects of classical slowing down and pitch angle scattering, stochastic diffusion associated with toroidal magnetic field ripple, and MHD activity. In order to separate the classical behaviour from the other effects, PCX measurements were obtained during MHD quiescent discharges in the plasma core region where stochastic ripple diffusion effects are negligible. This "plasma core" is taken to be the region well inside the boundary determined using the following expression provided by the Goldston-White-Boozer [32] theory:

$$\delta_{TF} \rho q' \left( \frac{\pi N q}{\epsilon} \right)^{3/2} \geq 1. \quad (12)$$

where  $\delta_{TF}$  is toroidal field ripple,  $\rho$  is the alpha gyro radius,  $N$  is the number of toroidal field coils,  $q$  is the safety factor,  $q' = dq/dr$ , and  $\epsilon$  is the inverse aspect ratio.

Plasma waveforms and pellet charge exchange signals illustrating a typical measurement scenario are shown in Fig. 2. All waveforms are diagnostic measurements except for the central alpha density, which is a TRANSP calculation. In the TFTR D-T experiments, pellets are injected 0.2 - 0.5 s after termination of neutral beam heating for PCX measurements. This timing delay leads to deeper penetration of the pellet as a result of decay of the plasma electron temperature and density as well as to an enhanced signal-to-noise ratio because the neutron background decays significantly faster than the confined alpha population. Note that at the selected time of pellet injection, the D-T neutron yield which gives rise to PCX signal interference has decayed by an order of magnitude while the alpha density remains virtually constant. A typical PCX signal along with the pellet light emission is shown at the bottom of the figure. The fluctuations on the neutral

signal are consistent with simple counting statistics, though some contribution from the time varying pellet cloud light emission [33] cannot be ruled out. Fluctuations on the particle signal do not correlate with the fluctuations on the light signal, which could occur if the ablation cloud remains an equilibrium thick neutralization target at all times. Uncertainties in the data points for the energy spectra and the radial profiles of the alpha signal due to these fluctuations typically range from  $\pm 10\%$  to  $\pm 50\%$  in going from lower to higher energy channels of the NPA. The light emission from the pellet ablation cloud is an indication of the lifetime of the pellet which typically burns out in  $< 2$  ms. No light signal is observed on the particle channels when the NPA electric and magnetic fields are nulled, so the particle signals are free of scattered light interference.

A key feature of all the PCX alpha signals is the delay in their rise relative to the light emission signal. In other words, we observe no alpha signal until the pellet penetrates to a certain plasma radius. The depleted region of the signal is observed in all discharges with PCX data. This behaviour is attributed to stochastic ripple loss depletion effects [17] in the outboard region of the plasma which the pellet must penetrate beyond before a measurable alpha population exists at the pitch angle viewed by the PCX diagnostic, as will be discussed further in Sec. 4.0.

## 2.1 Alpha Particle and Triton Energy Spectra

The alpha slowing down spectrum for a D-T discharge and the triton spectrum from a similar D-D discharge are shown in Fig. 3. The basic discharge parameters were:  $R_{\text{maj}} = 2.52$  m,  $a = 0.8$  m,  $P_b \sim 20$  MW with  $I_p$  ramped down from 1.7 MA to 1.0 MA during the 1.3 s duration neutral beam heating pulse. In going from alphas to tritons, the relevant values of the neutral equilibrium fraction, the ion velocity, and the analyzer detection efficiency associated with  $K(E)$  in Eq. 2 were employed. The midplane ripple diffusion boundaries for both 3.5 the MeV alphas and the 1.0 MeV tritons were identical to within 5% in these discharges, with a value of  $R = 2.76$  m. The energy spectra were measured in the ripple-free region inboard of this boundary. Note that the error bars in Fig. 3 only reflect the statistical errors due to the counting statistics.

Also shown are TRANSP (solid curves) and FPPT (dashed curves) predictions of the alpha and triton energy spectra. The absolute scale for  $dn/dE$  was derived from normalization of the PCX data with the TRANSP modeling results and was made only once for the alpha data as noted in the figure. The same normalization is used for the triton spectrum. Agreement between the PCX measurements and the spectra calculated by TRANSP is quite good, indicating that the alpha and triton energy distributions and their density ratio is close to the TRANSP prediction, which assumes classical slowing down and neoclassical alpha and triton confinement. For the FPPT simulations, the shape of the energy spectra is similar, but differences occur due to the fact that Coulomb scattering is included in TRANSP but not in FPPT, which has an effect that is particularly evident toward lower energies in the slowing down distributions. For the triton spectra



near the birth energy, the inclusion of a preliminary model for kinetic broadening in FPPT but not in TRANSP is the cause of the difference between the two simulations. Based on the agreement of the energy spectra and the alpha-to-triton ratio with TRANSP predictions, we infer that fusion generated-alphas and tritons in the core of MHD quiescent TFTR plasmas are well-confined and slow down classically.

To enhance the pellet penetration and also to increase the signal level at higher alpha energies, boron pellets were used in place of lithium [8]. For alpha energies above  $\sim 2$  MeV the calculated equilibrium fraction [18] for boron is significantly higher than for lithium. The higher heat of ablation energy of 5.3 eV/atom for boron compared with 1.6 eV/atom for lithium leads to an increase in the pellet penetration and consequently access a region of higher alpha density deeper in the plasma core. In practice, this gain is partially offset by lower pellet velocity from the injector due to the larger mass of boron relative to lithium. Nevertheless, under similar plasma discharge conditions an increase in the penetration for boron pellets ranging up to 20% ( $\sim 12$  cm) relative to lithium pellets of comparable mass is observed. In order to validate both the use of boron and the models used for alpha neutralization in pellet clouds, alpha energy spectra were compared for D-T discharges using both lithium and boron pellets [13]. The shapes of the measured alpha energy spectra for lithium and boron pellets were essentially the same, despite the very different energy dependence of the neutralization fractions used in their respective data analysis calculations.

The alpha distribution from 1.0 - 3.5 MeV was obtained using a single boron pellet injected 200 ms after termination of a 1.0 s beam pulse. The basic discharge parameters were:  $R_{\text{maj}} = 2.52$  m,  $a = 0.8$  m,  $I_p = 1.5$  MA,  $B_T = 5.2$  T and  $P_b = 16$  MW. The alpha energy spectrum obtained from the PCX measurements for this discharge is shown by the solid circles in Fig. 4. Also shown (solid squares) is the energy spectrum measured for a "beam blip" case ( $P_b = 20$  MW), where the boron pellet was injected 20 ms after a beam pulse of only 100 ms duration. The curves are the FPPT simulations of the PCX measurements. Reasonable agreement is seen between the data and the FPPT code results, which indicates that the alpha particles slow down classically. In addition, the absence of any peaking in the fully developed slowing down spectra in the region of 3.5 MeV indicates that massive prompt losses do not occur. This is consistent with the alpha particles being well confined. Experimental results from the  $\alpha$ -CHERS [34] and the escaping alpha [35] diagnostics on TFTR, both of which are absolutely calibrated, corroborate this classical picture of alpha behaviour and also show that massive prompt losses of alphas do not occur in MHD-quiescent plasma discharges.

In the "beam blip" discharge, the alphas are created in a time interval short compared to the alpha slowing-down time. In principle, the measured energy spectrum for this short pulse neutral beam injection scenario can potentially yield information on the alpha birth energy distribution. Unfortunately, the existing TRANSP code does not provide for modeling of the kinetic spreading of the alpha birth energy spectra, which must include precise information about beam energies

species and injection angles, the computed thermonuclear beam-plasma and thermonuclear mix, and the ion temperature. In the FPPT code, a preliminary model of the "beam blip" data assumes simple thermonuclear Doppler broadening of the alpha particle birth energy,  $E_\alpha$ , for which the full width at half maximum is given approximately by  $\Delta E(\text{keV}) = 182(T_{\text{eff}})^{0.5}$  where  $T_{\text{eff}} = 30$  keV, the mean effective temperature of the deuterium and tritium ions, is based on measurement of the D-T neutron broadening in TFTR using a natural diamond spectrometer [36].

For the discharges used in this work, the alpha population is sufficiently dilute that single-particle behaviour is expected. To date, no 'anomalous' alpha particle losses due to alpha-driven collective instabilities have been observed in TFTR NBI-heated D-T discharges without ICRH [1, 35]. This fact supports the assertion that the PCX alpha and triton measurements indicate that the alpha and triton behaviour is classical.

The alpha slowing down spectrum in Fig. 4 can be modeled to derive information on the alpha confinement time. For this purpose, the drift-averaged Fokker-Planck equation used in the FPPT code (Eq. 5) was modified as follows :

$$\partial f_\alpha / \partial t = \langle St(f_\alpha) \rangle + \langle S_\alpha \rangle - f_\alpha / \tau_\delta - f_\alpha / \tau_{\text{conf}} \quad (13)$$

where  $f_\alpha$  is the distribution function of alphas including the thermal broadening effect,  $St(f_\alpha)$  is the collisional integral describing the slowing down of alphas,  $S_\alpha$  is the alpha source taken from TRANSP code,  $\tau_\delta$  is the confinement time of alphas determined by the effect of toroidal field ripple, and  $\tau_{\text{conf}}$  is the confinement time of alphas determined by alpha radial transport of any other type excluding ripple effects. Fig. 5 shows same data for the energy spectrum of alphas during the slowing down phase as shown in Fig. 4. The alpha slowing down time in this case is equal to  $\tau_{\text{sl}} = 0.32$  s. The solid line shows the FPPT calculation assuming that  $\tau_{\text{conf}} \gg \tau_{\text{sl}}$ ; i.e.  $\tau_{\text{conf}} = 300 \tau_{\text{sl}}$ . The broken lines present the cases where  $\tau_{\text{conf}} / \tau_{\text{sl}} = 3.0, 1.5, 0.8$  and  $0.4$ . In comparison with the FPPT simulation, the PCX alpha slowing down spectrum is consistent with an alpha confinement time of  $\tau_{\text{conf}} > 3.0 \tau_{\text{sl}}$ . This again supports the assertion that the alpha particles thermalize classically, which is important for good alpha heating in a fusion reactor.

## 2.2 Alpha Radial Profiles in Supershot Discharges

The alpha differential density profile was measured in the core of MHD-quiet supershot discharges using the PCX diagnostic. Fig. 6 presents radial profiles of alphas with energies of 0.64, 0.8, 1.0, 1.21 and 1.41 MeV measured 0.3 s after termination of 20 MW beam

injection, normalized at  $R = 2.65$  m. Also shown are the Goldston-White-Boozer (GWB) stochastic ripple diffusion radial boundary corresponding to alpha energies of 0.64, 1.41, and 3.5 MeV. Inside the GWB boundaries the alpha behaviour is classical while outside there exists a domain where alpha particles are strongly affected by stochastic ripple diffusion. It is seen that alpha density profiles are consistent with the GWB boundary for  $E_\alpha = 3.5$  MeV. This demonstrates the absence of significant alpha transport outward during slowing down from the birth energy to at least 0.64 MeV and the strong ripple influence on alphas outside the GWB boundary. Ripple diffusion causes alphas born outside the GWB boundary to be promptly lost while alphas born inside this boundary are confined and slowing down there in the absence of any outward transport. Note that at the time of measurement (0.3s after the termination of neutral beam heating) the generation of alphas is practically absent. Fig. 7 presents the experimental radial alpha profiles and the FPPT code predictions for  $E_\alpha = 0.64$  MeV and 1.21 MeV with and without ripple. Modeling results are normalized to the PCX data separately for both energies. It is seen that experimental data are in good agreement with the ripple modeling. Fig. 8 shows the corresponding energy spectra with and without ripple. It is seen also that the modeling without ripple predicts much broader radial density profiles and steeper energy spectra than experimentally measured.

The PCX radial profiles of the alpha signal such as those shown in Fig. 6 can be analyzed to obtain information on the radial transport of trapped alpha particles. However, the FPPT code is based on the method of integration over the particle characteristics [29], which does not allow inclusion of the second derivative operator. Thus, FPPT does not have pitch angle scattering in the collisional operator, which results in radial transport, and therefore the FPPT code cannot treat the diffusion self consistently. Nevertheless, a diffusive type equation can be constructed within the FPPT formalism to model radial diffusion [28]. The results of this procedure are shown in Fig. 9 for a fixed alpha particle energy of  $E_\alpha = 1.2$  MeV. It can be seen that the best fit to the measured PCX profile occurs for the smallest diffusion value,  $D_\alpha < 0.01$  m<sup>2</sup>s<sup>-1</sup>, which indicates that there is no significant radial transport. Similar results have also been obtained in TFTR D-T plasmas using the  $\alpha$ -CHERS diagnostic [4]. This diagnostic is sensitive primarily to passing alphas, whereas the PCX views only trapped alphas. In the  $\alpha$ -CHERS case, modeling of the spatial alpha profile measurements constrained the anomalous alpha radial diffusivity in addition to neoclassical transport to values less than  $D_\alpha = 0.03$  m<sup>2</sup>s<sup>-1</sup> [37]. The small values obtained by both the PCX and  $\alpha$ -CHERS diagnostics are consistent and are comparable to the neoclassical diffusivity.

### 2.3 Alpha Radial Profiles in Reversed Shear Discharges

In monotonic shear in the absence of any MHD activity, the radial profiles of alphas measured by the PCX have similar shapes defined by the source function and the ripple losses for generated alphas. In reversed shear discharges which characteristically have an elevated central  $q$ -

factor, the measured alpha radial profiles of higher energy ( $\sim 1.7$  MeV) alphas appeared to be significantly broader than for lower energy ( $\sim 0.5$  MeV), as shown in Fig. 10. High  $q(0)$  decreases the stochastic threshold, as is evident from Eq. 12. As discussed below, enhanced stochastic ripple loss of the alphas under these conditions appears to be the cause of this behaviour.

The ORBIT guiding center code calculates alpha guiding center orbits in flux coordinates for real magnetic geometry, including pitch angle scattering, slowing down and toroidal precession for fast ions. Calculations of the toroidal ripple loss have been made for alpha particles in a reversed shear plasma [38] using an enhanced version of the ORBIT code [39] which utilizes a rapid, accurate algorithm for the stochastic free domain. Figure 11 shows the confined domains for the reversed shear and high current monotonic shear scenarios as a function of alpha particle energy. Confinement, with bounded periodic bounce tip motion and no stochastic ripple loss, is predicted for trapped alpha particles whose bounce points lie in the shaded regions shown in the figure. At the alpha particle birth energy of 3.5 MeV, the stochastic diffusion loss region occupies the whole plasma in the TFTR reversed shear plasma equilibrium. All trapped particles are quickly lost through first orbit or stochastic ripple diffusion. Passing alpha particles slow down and are pitch angle scattered into trapped orbits, for which there are confinement regions at lower energies. At high energies the confinement domains cover less of the plasma cross section in reversed shear than in the monotonic shear comparison case. As an ion slows down, the shaded confinement domain increases so that at thermal velocities no stochastic ripple loss is predicted and neoclassical and anomalous losses predominate.

ORBIT was used to model the PCX results obtained during reversed shear operation [40]. Alpha particles with initial profiles consistent with the Abel-inverted neutron profiles measured on TFTR were followed for  $\tau_S$  and  $2\tau_S$  in both monotonic and reversed magnetic shear geometries. The simulated profiles are compared to PCX results for monotonic and reversed shear cases in Fig. 12. In monotonic shear, the profiles at  $\tau_S$  (1.3 MeV) and  $2\tau_S$  (0.5 MeV) are similar to those observed by PCX. The simulated profile at 0.5 MeV extends over a larger region in  $r/a$  as expected from the larger stochastic free region at lower energy. In reversed shear, two features of the PCX measurements are distinctly different from the monotonic shear case: 1) a flat or hollow distribution at 1.71 MeV, which appears to be filled as the energy of the observed alphas decreases to 1.3 MeV and 0.5 MeV; 2) a very steep profile at 0.5 MeV. The model predicts the general characteristics of alpha loss in reversed shear which clarify how a hollow profile could arise. In reversed shear, no trapped alphas would be observed at 3.5 MeV, while at lower energies a peaked, flat or hollow profile can result depending on pitch angle scattering and the passing alpha distribution. In ongoing work, other simulations made with significant variations in the pitch angle scattering rate show that the results of Fig. 12 are not sensitive to this parameter. Since the simulation error bars are comparable to those of the measurements, neoclassical modeling with ORBIT gave good agreement with both the monotonic and reversed shear measurements.

### 3.0 PCX MEASUREMENTS IN THE PRESENCE OF MHD ACTIVITY

MHD activity (e.g. sawtooth oscillations and TAE activity) can transport alphas from the plasma core which might affect ignition and/or damage of the first-wall components of the vessel by feeding the alphas into the stochastic ripple loss region. In D-T experiments on TFTR, the behaviour of fast confined alphas in the presence of sawtooth activity was measured using the PCX and the  $\alpha$ -CHERS diagnostics. Both diagnostics have observed evidence for sawtooth redistribution of confined alphas by sawtooth crashes [4, 14-16] and show a strong depletion of the alpha core density and transport of the alphas radially outwards well beyond  $q = 1$  surface after a sawtooth crash. Lost alpha detectors measure bursts of alpha loss coincident with sawtooth crashes [41] which represent a very small fractional loss of the previously confined alphas (<1%). Thus, a sawtooth crash leads mainly to radial redistribution of the alphas rather than losses. In addition, PCX measurements have been obtained in discharges in which TAE activity occurs in conjunction with reduced shear operation.

#### 3.1 Alpha Redistribution due to Sawtooth Oscillations

This section presents the PCX measurements and modeling of alpha redistribution due to sawtooth oscillations. The experiments were performed in standard TFTR D-T supershots [1] with a plasma current of 2.0 MA, a toroidal magnetic field of 5T, major and minor radii of  $R = 2.52$  m and  $a = 0.87$  m and 20 MW of DT neutral beam power injection. Sawteeth do not normally occur during beam injection in these supershots. However, large sawteeth begin to develop 0.2 - 0.3 s after the termination of beam injection, as shown in Fig. 13, when the plasma  $\beta$  drops below the level required to suppress sawteeth. To obtain PCX data, a Li pellet was injected before and after the sawtooth crashes in sequential similar discharges. Measured radial profiles for alpha energies of 0.64 MeV and 1.21 MeV before and after the crash are shown in Fig. 14. The alphas are depleted in the core and redistributed to well outside the  $q = 1$  radius, but are not observed beyond the stochastic ripple loss boundary corresponding to the alpha energy being measured. The broadening decreases with increasing energy, as does the radius of the stochastic ripple loss boundary.

Models of the effect sawtooth oscillations on confined fast ions [42] were developed for neutral beam injected passing particles having small radial deviations from the magnetic surface. This magnetic reconnection formalism was used to model the  $\alpha$ -CHERS data for fast particle redistribution [43]. A small radial diffusion coefficient  $D_{\alpha} = 0.03 \text{ m}^2\text{s}^{-1}$  in addition to neoclassical was introduced after the sawtooth crash to fit the data. The agreement of the model with the experiment data indicates that energetic passing alphas redistribute with the magnetic flux.

The crash time is sufficiently short that the induced electric field can modify the particle distribution through resulting ExB drift [28, 44 - 45]. The effect on the trapped alpha particle orbits of the magnetic reconnection and ExB drift is illustrated in Fig. 15. Note that the PCX diagnostic views alphas on the counter-going (inner) leg of the trapped orbits. The perturbed helical electric field provides significant alpha displacement along the major radius.

A model based on this approach was incorporated in the FPPT code for simulation of the sawtooth redistribution observed by the PCX diagnostic. A helical electric field,  $E_{r,\theta}$ , is assumed to be generated during the so-called "collapse" period of the sawtooth oscillation on a very short time scale  $\tau_{cr} \sim 10^{-5} - 10^{-4}$  s where  $\tau_{cr}$  is the crash time. This electric field leads to a change of the alpha energy due to the toroidal drift motion,  $v = cE_{r,\theta}xB/B^2$ . We acknowledge that the time scales may be on the edge of applicability for the bounce-averaged equations [45]. However, for well trapped particles the analysis may remain valid since the orbit bounce points do not extend far from the midplane. In order to model sawtooth redistribution in FPPT, we introduced a simple analytical transformation formula for alpha particle energy redistribution which was shown to obey a diffusion type of equation [28]. In this approach, particles can undergo significant displacement within the alpha mixing radius during the crash. The interaction of the fast particles with the perturbed electric field can be considered as resonant, even though the mode itself has very low frequency and was assumed not to be rotating during the short crash. Therefore, particles with energy higher than some critical value  $E_{cr}$  perform toroidal precession during the crash and do not interact with perturbed electric field. This critical energy,  $E_{cr} = 2\omega_c m_\alpha r R / \tau_{cr}$ , is defined [45] from comparison of the particle toroidal precession time and the sawtooth crash time, where  $\omega_c$  is the cyclotron frequency,  $m_\alpha$  is the alpha particle mass, and  $r$ ,  $R$  are the minor and major radii, respectively.  $E_{cr}$  plays the role of an adjustable parameter in simulations of the experimental data as discussed below and avoids the need for precise knowledge of the crash time  $\tau_{cr}$ .

Figure 16 illustrates the procedure used to determine the adjustable parameter,  $E_{cr}$ , used in application of the model including ExB drift of the alphas to the experimental PCX data for sawtooth mixing of trapped alphas. The PCX experimental points are shown as solid circles. The pre crash curve is normalized to the PCX data for a similar shot without sawteeth. One can see from profile comparisons that  $E_{cr}/E_{\alpha 0} = 1$  gives the best fit to the data. In all the calculations, a mixing radius [46] of  $r_{mix} = 1.5r_s$  ( $q(r_s) = 1$ ) was used. The value of  $r_{mix} = 1.5r_s$  is about the sawtooth mixing radius for the bulk plasma and yields the best fit to the PCX data.

Figure 17 shows the comparison of the PCX data with the sawtooth redistribution model for a measured alpha energy of 1.21 MeV. Within the accuracy of the PCX measurements and the model, good agreement is seen in comparisons of the experimental alpha radial profile and the model. The application of this model to the passing particles does not produce alpha redistribution because of the very fast toroidal rotation of those particles.

Comparison of the PCX and  $\alpha$ -CHERS data with lost alpha measurements shows that in the sawtooth crashes, radial redistribution of the alphas occurs without significant ripple losses of particles. The sawtooth oscillations effectively transport the alphas outward along the major radius close to the stochastic ripple domain. Under conditions of larger mixing radius than occurs in TFTR, this transport might lead to enhanced ripple loss of fusion alpha particles in tokamaks.

### 3.2 Alpha Redistribution in the Presence of TAE Activity

Recently  $\alpha$ -TAE modes have been observed in deuterium-tritium plasmas in TFTR [47]. These modes are observed 100-200 ms following termination of neutral beam injection in plasmas with reduced central magnetic shear and elevated central safety factor [ $q(0) \sim 2$ ]. Mode activity is localized to the central region of the plasma ( $r/a < 0.5$ ) with weak magnetic fluctuation levels of order  $\text{dB/B} < 10^{-4}$  Gs and toroidal mode numbers in the range  $n = 2 - 4$ .

The scenario for measurement of alpha distributions in the presence of TAE activity is illustrated in Fig. 18. TAE activity typically occurred  $\sim 150$  ms after termination of beam injection. The PCX measurements were performed in the range of  $100 \pm 50$  ms after TAE activity ceased. Radial profiles of the alpha signal at different energies in the presence of TAE modes ( $n = 3$ ,  $\text{dB/B} = 2.10^{-4}$  Gs) are shown in Fig. 19. The data were taken in a single shot (#94001) having plasma current 1.7 MA, NB power 25 MW,  $q(0) = 2.35$  and a flat  $q(r/a)$  profile. The PCX measurements were performed 150 ms after TAE modes. The solid curves are experimental data, while the dashed curves are similar discharges without TAE activity. With TAE activity, the redistribution becomes broader and more depleted in the core with increasing alpha energy.

In Fig. 20, the thick curves show the alpha energy spectra measured by PCX 150 ms after the TAE in the plasma center ( $r/a = 0.02$ ) and for a more outboard position ( $r/a = 0.38$ ). Classical predictions for these radial positions are shown by the thin curves. It is seen that in central position there is a depletion of particles with the energy  $E_\alpha > 1.5$  MeV than the classical model predicts. On the contrary, in the outside position ( $r/a = 0.38$ ) the number of alphas having  $E_\alpha > 1.2$  MeV is much higher than for the classical case.

In view of the weak magnetic fluctuation levels attending the core TAE activity, it is natural to question how this can produce the significant modifications of the alpha energy spectra and radial distribution observed by the PCX diagnostic. In the modeling approach described below, we argue that only a very small change in the alpha energy due to interaction with the TAE mode is needed to cause displacement of the trapped alpha orbit from the narrow pitch angle window viewed by the PCX diagnostic and lead to the observed redistributions.

To provide a simplified illustration of the  $\alpha$ -TAE behaviour, consider the zero banana width resonance condition,

$$\omega - \langle \omega_d \rangle - \langle k_{\parallel} v_{\parallel} \rangle = 0 \quad (14)$$

where  $\omega$  and  $\omega_d$  are the TAE and particle precession frequencies, respectively,  $k_{\parallel}$  is the mode wave vector and  $v_{\parallel}$  is the particle parallel velocity. For trapped particles, the resonance condition can be approximated by

$$\frac{\langle \omega_d \rangle}{\omega} \cong \frac{nq^2 v_{\perp} \rho_{\alpha}}{\varepsilon v_A R} F(\chi) \quad (15)$$

where  $n$  is the toroidal mode number,  $q$  the local safety factor,  $v_{\perp}$  particle perpendicular velocity,  $\rho_{\alpha}$  the alpha Larmor radius,  $\varepsilon$  the inverse aspect ratio,  $v_A$  the local Alfvén velocity and  $R$  the major radius.  $F(\chi)$  is a function of particle pitch angle which is approximately unity for deeply trapped alphas. Figure 21 shows the  $\alpha$ -TAE resonance for a typical discharge with core TAE activity on TFTR where  $\rho_{\alpha}/R = 0.02$ ,  $\varepsilon = 0.1$ ,  $v_{\alpha 0}/v_A = 0.7$ ,  $n = 3$  with  $q$  values as shown on the figure. Note that lower  $q(0)$  leads to resonances at higher alpha energies and that for  $q(0) < 1.45$ , the resonance no longer intersects the alpha distribution. This is consistent with the fact that the PCX diagnostic only observes significant alpha redistribution in the presence of TAE activity when the safety factor approaches  $q = 2$ .

A more accurate analysis of the resonance condition of trapped alphas during their interaction with TAE modes was performed which includes finite banana width effects. As before, the alpha particles are in fundamental resonance with the mode when  $q(0)$  is sufficiently large, typically  $q(0) > 2$  for the  $n = 3$  mode. Furthermore, the analysis showed that near the plasma center the resonance is very broad for trapped alphas in terms of their vertical displacement. This means that trapped particles in the resonance zone can be displaced vertically and lost from the PCX pitch angle viewing window. Restricting the particle deviation from the resonance condition,  $(\Delta f/f)_{\text{TAE}}$ , to a small value enables a rough estimate of the possible particle displacement to be obtained. Such a scenario is illustrated in Fig. 22, where particle displacement is predicted in a zone with a vertical extent of  $\Delta Z \sim 0.3$  m. This TAE resonance zone corresponds to  $E_{\alpha} = 2 - 3$  MeV,  $v_{\parallel}/v = -0.05$ ,  $q(0) = 2.2$ , and  $(\Delta f/f)_{\text{TAE}} = 0.01$ . In this figure, orbit A is for  $E_{\alpha} = 3.5$  MeV with the pitch angle  $-0.05 \pm 0.001$  which becomes orbit B after the interaction with  $\alpha$ -TAE resonance zone. This orbit is located in the ripple confinement domain [39] but out of the PCX pitch angle window. Orbit B can be slow down to the energy  $E_{\alpha} = 1.7$  MeV and pitch angle scatter during  $\sim 150$  ms after TAE mode, yielding orbit C which is again within the PCX pitch angle window and be detected. Alternatively, the vertical drift of alpha orbit bounce point due to the TAE interaction may shift alphas into the stochastic ripple loss domain, whose boundary is



relatively close to the top of the  $\alpha$ -TAE resonance zone. Other alpha orbits having energy  $\sim 2$  MeV which remain in the pitch angle range  $0 - 0.2$  can also slow down and scatter during  $\sim 150$  ms time interval after TAE to refill the PCX pitch angle window and be detected by the PCX at the major radius  $2.8 - 3.0$  m. Detailed modeling of this proposed mechanism to numerically simulate the PCX measurements, including the possible effects of stochastic ripple diffusion loss, is in progress.

#### 4.0 STOCHASTIC RIPPLE EFFECTS

The primary mechanisms of toroidal field (TF) ripple induced fast ion transport are direct ripple trapping, ripple plateau diffusion, ripple banana diffusion, and stochastic ripple diffusion. In direct ripple trapping, the toroidal field ripple creates secondary magnetic wells that can trap superbanana particles and cause them to drift vertically until they strike the vessel wall. Collisionless stochastic ripple diffusion occurs when the field ripple induces a random radial step of the banana orbit, mainly near the bounce point where the parallel velocity of the particle is small. When the banana tip displacement is sufficiently large to make the toroidal angle change between successive bounce points larger than the toroidal period  $\frac{2\pi}{N}$  ( $N$  = the number of TF coils) the radial steps become decorrelated, randomizing the motion, and diffusive loss of particles takes place. Assuming conservation of energy and magnetic moment, the banana tip moves vertically in a random walk fashion until the particle strikes the vessel wall. The onset of stochastic motion cannot be accurately predicted by present day theory; however, a simplified analytical approximation for the stochastization threshold can be expressed as:

$$\frac{2\delta_{\text{TF}}\rho q'}{\pi} \left( \frac{\pi N q}{\epsilon} \right)^{\frac{3}{2}} \left( \frac{\theta_b + S^{-1} \cot \theta_b}{\sqrt{\sin \theta_b}} \right) \geq 1, \quad (16)$$

where  $\delta_{\text{TF}}$  is the magnetic field ripple,  $\rho$  the particle gyroradius,  $\epsilon$  the inverse aspect ratio,  $q$  the safety factor,  $q' = \frac{dq}{dr}$ ,  $S = r \frac{q'}{q}$  the magnetic shear and  $\theta_b$ , the poloidal angle of the bounce point. Equation 16 is the midpoint of the 'fuzzy' stochastic boundary that corresponds to  $\alpha = \sqrt{2}$  (see Eq. 11). Note that in the limit of  $\theta_b = \frac{\pi}{2}$ , Eq. 16 reduces to the familiar Goldston-White-Boozer (GWB) threshold given in Eq. 12. PCX measurements were used to examine the functional dependence of the stochastic ripple threshold as expressed in Eq. 16. Several key plasma parameters can change the ripple threshold. Two parameters of interest are the safety factor  $q$  and its radial derivative  $q'$ . Experimentally  $q$  and  $q'$  can be modified by varying the plasma current on TFTR.

The PCX diagnostic measures trapped alpha particles with very small pitch angle ( $v_{||}/v = -0.048$ ) at the midplane, which are very sensitive to toroidal magnetic field ripple. Figure 23 is a mapping of the 3.5 MeV alpha loss boundary in pitch angle and major radius space for a 1.4 MA TFTR supershot discharge. The figure is the result of an orbit following calculation using the Hamiltonian formalism developed by White et al. [48]. The code imposes a vacuum field ripple  $\delta$  onto an axisymmetric poloidal field given by a MHD equilibrium. The field ripple  $\delta$  takes the same form as that used in the FPPT code. The pitch angle and major radius scan is produced by following the 3.5 MeV alpha particle guiding center in the "TF-rippled" equilibrium for an alpha slowing down time. Simulations were performed without ripple (first orbit loss only), with ripple, and with ripple and collisionality. From the figure, we can see that TF ripple opens up a loss region for perpendicular orbits. The addition of collisionality essentially widens the loss region, particularly with midplane  $\frac{v_{||}}{v} \sim 0$ . The PCX diagnostic, in its current geometrical configuration, provides a radial scan at  $\frac{v_{||}}{v} \sim -0.048$  on this map. This simulation produces a snap shot of the alpha loss boundary and can only be used for qualitative comparisons with the PCX data. However, the comparison provides an excellent guide in understanding the physical cause for the depletion of PCX alpha signal near  $\frac{v_{||}}{v} \sim 0$ .

A comparison between the stochastic ripple boundary from the PCX and from the GWB formalism at different plasma currents for sawtooth-free discharges is shown in Fig. 24. During pellet penetration, the rise of the PCX alpha signal is delayed relative to the pellet light emission as illustrated by the insert. The delayed rise correlates with the pellet crossing inside the ripple loss boundary for the trapped ions viewed by the PCX spectrometer. In quiescent discharges, where there is no radial redistribution of the alphas due to sawteeth activity, the ripple boundary is determined by the birth alpha energy. Experimentally, we observe the signals from all the PCX alpha energy channels appearing at approximately the same radial location. Even though lower energy alphas have ripple loss boundaries at larger radii, there is no source of these lower energy alphas outside the 3.5 MeV boundary because the alphas born outside this boundary are lost before they can slow down. Hence the boundary for all energy alphas is determined by the ripple boundary at birth energy.

The plasmas used for this data set were TFTR D-T supershot discharges with 5.0 Tesla toroidal field. The plasma current varied from  $I_p = 1.3 - 2.0$  MA; there were two data points where the current was ramped up from 0.6 to 1.4 MA (solid diamond) and ramped down from 2.2 to 1.4 MA (solid circle). The plasma major radius is  $R = 2.52$  m except for the 1.5 MA discharge where  $R = 2.45$  m. The peak electron densities were about  $5.0 \times 10^{19} \text{ m}^{-3}$  for the constant current discharges and  $2.0 \times 10^{19} \text{ m}^{-3}$  when the current was ramped. The peak electron temperatures ranged from 8 to 16 keV for the constant current cases and was approximately 5 keV for the

current ramps. The plasmas were heated by a mixture of deuterium and tritium neutral beam injection ranging from 7 MW to 20 MW. The peak DT neutron emission was about  $1.2 \times 10^{18} \text{ s}^{-1}$  for constant currents and  $1.4 \times 10^{17} \text{ s}^{-1}$  for ramped currents.

Within the noted plasma current range, the measured ripple boundary varied by about 10 cm. The corresponding toroidal field ripple amplitude increased by about 40% from  $1.8 \times 10^{-4}$  to  $3.0 \times 10^{-4}$  Tesla. The comparison indicates that the measured boundaries are varying with  $q$  and  $q'$  consistent with the scaling predicted by the Goldston-White-Boozer theory. However the measured boundaries consistently occur at smaller major radii than the theoretical prediction. On the average, the difference is  $\sim 6$  cm. Such difference is not too surprising since the GWB criterion only provides an estimate of the stochastization threshold at which the particles are rapidly expelled and does not include finite orbit effects. In practice, the ripple boundary need not be a sharp transition but a soft boundary described by finite diffusive process.

In order to examine the dependence of the ripple boundary on the alpha energy, PCX measurements were made following the large sawteeth that occur during the post neutral beam heating phase of TFTR discharges. As discussed in Sec. 3.1, sawtooth activity produces radial transport of alphas. Hence, when the alpha distribution is measured after sawtooth instabilities, observe alpha particles are observed outside the birth energy ripple boundary. These particles will then be confined based on the ripple boundary appropriate to their energy. Under these conditions, the PCX measured alpha signals in different energy channels now appear at different radial locations which should reflect the stochastic ripple boundaries corresponding to their respective energies. Figure 25 shows the PCX measured ripple boundary for different alpha energies after sawtooth instabilities for two similar discharges. Over the available energy range of the measurements ( $E_\alpha = 0.53 - 1.21$  MeV), the experimental data have the same functional energy dependence as the GWB ripple model. As was the case for the results given in Fig. 24, the measured boundaries again occur at smaller major radii than the predicted boundary. A possible contributing factor is that the data are taken after post beam sawteeth where the  $q$  profile is not known with good accuracy. As a result, the predicted ripple boundary may be somewhat too large. Another possible explanation of the difference between measurement and theory may be that in the GWB analysis, the effect of slowing down has not been taken into account. This can be an important factor since the data are taken approximately 120 ms after the sawtooth crash, which is comparable to the alpha slowing down time. The hatched points in Fig. 25 show the effect of regressing the alpha energy back from the measured value to the energy at the time of the sawtooth crash.

## 5.0 RF-DRIVEN TRITIUM ION TAILS

Although this paper primarily addresses the behaviour of confined trapped alphas, observations of energetic RF-driven ions are also of interest. The energy spectra of RF-driven minority ion tails RF-driven minority tail ions were measured on TFTR using the PCX diagnostic, including  $^3\text{He}$  spectra using active analysis with Li pellets [9] and H spectra using both active and passive methods [10].

Active PCX measurements of the energy spectrum, differential radial density distribution, and heating deposition profile of RF-driven tritium ions during  $2\Omega_T$  heating of low-beta, L-mode D-T plasmas [49] also were made. During these experiments, the energy spectrum and radial profile of the effective temperature of the tritium tail were obtained using PCX. The basic discharge parameters were:  $R = 2.63$  m,  $a = 0.9$  m,  $I_p = 1.8$  MA and  $B_T = 5$  T. The PCX tritium signals as a function of major radius for  $E_{\text{Tritium}} = 0.27\text{-}0.86$  MeV are shown in Fig. 24. The measurement was made during the 2.8 s flattop phase of the 1.8 MA D-T discharge. The tritium content of the target plasma was about 50%. The RF heating was applied from 2.8 - 4.5 s and reached a launched power of  $P_{\text{rf}} = 2.75$  MW, but dropped to 1.5 MW from 3.2 - 4.5 s due to a fault. The Li pellet was injected at 4.4 s near the end of the RF pulse. At the time of pellet injection, the central electron temperature and density were approximately 2.9 keV and  $3.8 \times 10^{19} \text{ m}^{-3}$ , respectively. The pellet penetrated slightly beyond the magnetic axis ( $R_{\text{axis}} = 2.74$  m). A large increase in the signal level occurred just inside  $R = 2.95$  m which is about 15 cm outboard of the ICRH resonance layer. The modulations in the PCX signals in Fig. 26 are observed on all energy channels. It is important to note that these modulations reflect a similar time variation in all energy channels and do not affect the energy spectrum. We believe that these fluctuations may be the result of the spatial variation in the density of the RF-driven tritium tail.

The energy spectrum near the resonance surface is shown in Fig. 27. A straight line fit to the measured energy distribution of the tritium tail yields an effective tritium tail temperature which is plotted as a function of major radius in Fig. 28. Preliminary results indicate that the formation of the tail is quite fast; the energy spectrum of the tail is fully developed after the first 100 ms of RF heating. Furthermore, the energy confinement time in these tritium discharges is similar to that seen in D-T plasmas heated by hydrogen minority ICRH. The tail temperature profile exhibits a transition near  $R = 3.0$  m where the effective temperature increases by a factor of two. The tritium density and tail temperature radial profiles suggest that most the heating occurs within 20 cm from the resonance surface.

## 6.0 SUMMARY

With the advent of D-T plasma operation on TFTR, a growing body of results from the PCX and other TFTR alpha particle diagnostics is providing important information about alpha particle behaviour. Using the PCX diagnostic, the first measurement of the alpha slowing down distribution up to the 3.5 MeV birth energy was obtained using boron pellet injection. In the core of MHD-quiescent D-T supershot discharges in TFTR, the good agreement observed between the PCX measurements of the confined, trapped alpha particles and tritons and TRANSP and FPPT predictions is consistent with the alphas and tritons being well confined and slowing down classically. In these monotonic shear supershots, the radial profiles of the alpha signal are centrally peaked and their shape does not depend on energy. On the other hand, in reversed shear discharges the radial profile shapes are energy dependent and exhibit a particle depletion in the core and profile broadening with increasing alpha energy. ORBIT code modeling indicates that this behaviour is caused by stochastic ripple loss effects resulting from the elevated central q-factor in such discharges. Significant redistribution of the radial profile of the alpha signal in the presence of strong sawtooth activity was observed wherein alphas are depleted in the core and redistributed to well beyond the  $q = 1$  radius. A sawtooth model based on alpha redistribution due to ExB drift which was incorporated in the FPPT code provided reasonable simulation of the PCX measurements. Redistribution of trapped alphas was also observed in the presence of core TAE activity with elevated central safety factor,  $q(0) \sim 2$ , and modeling of these measurements based on an  $\alpha$ -TAE resonance mechanism is in progress. Stochastic ripple loss effects were studied and the PCX results agree with the energy and q-factor scaling of the Goldston-White-Boozer theory. Measurements of the radial profile and energy spectrum of the tritium tail during ICRH heating of an L-mode plasma at the second harmonic tritium cyclotron frequency were obtained. The PCX data showing formation of an energetic tritium ion tail provide evidence of ion heating, and in combination with diamagnetic data showing a substantial increase in the thermal stored energy in TFTR, support the idea of using second harmonic ion cyclotron heating as a viable technique for heating the relatively cold, low density ITER startup plasma [50].

## ACKNOWLEDGEMENTS

This work was supported by US DoE Contract DE-AC02-76-CHO-3073 and US DoE Grant DE-FG03-92ER54150.

**REFERENCES**

- [1] HAWRYLUK, R. J. "Results from Deuterium-Tritium Tokamak Confinement Experiments," To be published in Reviews of Modern Physics, April 1998.
- [2] HEIDBRINK, W. W. and SADLER, G., Nucl. Fusion **34** (1994 ) 535.
- [3] ZWEBEN, S. J., et al., Plasma Phys. Control. Fusion **39** (1997) A275.
- [4] STRATTON, B. C., et al., Rev. Sci. Instrum. **68** (1997) 269.
- [5] WOSKOV, P. P., et al., Rev. Sci. Instrum. **59** (1988) 1565.
- [6] FISHER, R. K., et al., Fusion Technol. **13** (1988 ) 536.
- [7] FISHER, R. K., et al., Rev. Sci. Instrum. **63** (1992) 4499.
- [8] MEDLEY, S. S., et al., Rev. Sci. Instrum. **67** (1996) 3122.
- [9] MEDLEY, S. S., et al., in Controlled Fusion and Plasma Physics (Proc. 20th Eur. Conf. Lisbon, 1993), Vol. 17C, Part III, European Physical Society, Geneva (1993) 1183.
- [10] McCHESNEY, J. M., et al., Rev. Sci. Instrum. **66** (1995) 348.
- [11] DUONG, H.H., et al., Rev. Sci. Instrum. **68** (1997) 340.
- [12] FISHER, R. K., et al., Phys. Rev. Lett. **75** (1995) 846.
- [13] MEDLEY, S. S., et al., Plasma Phys. Control. Fusion **38** (1996) 1779.
- [14] PETROV, M. P., et al., Nucl. Fusion **35** (1995) 1437.
- [15] PETROV, M. P., et al., in Proc. of the 16th IAEA Fusion Energy Conference Montreal, 1996 (International Atomic Energy Agency, Vienna, 1996) Paper IAEA-CN-64/A2-2.
- [16] PETROV, M. P., et al., in Controlled Fusion and Plasma Physics (Proc. 23rd Eur. Conf. Kiev, 1996), Vol. 20C, Part I, European Physical Society, Geneva (1996) 63.
- [17] DUONG, H.H., et al., Nucl. Fusion **37** (1997) 271.
- [18] McCHESNEY, J. M., et al., Phys. Plasmas **4** (1997) 381.
- [19] KISLYAKOV, A. I., et al., Fusion Engineering and Design **34-35** (1997) 107.
- [20] BUDNY, R. V., Nucl. Fusion **34** (1994) 1247.
- [21] REDI, M. H., et al., Nucl. Fusion **35** (1995) 1509.
- [22] CAVALLO, A., et al., Rev. Sci. Instrum. **59** (1988) 889.
- [23] MANSFIELD, D. K., et al., Appl. Opt. **26** (1987) 4469.
- [24] BUSH, C. E., et al., Rev. Sci. Instrum. **66** (1995) 1193.
- [25] LEVINTON, F. L., Phys. Rev. Lett. **75** (1995) 4417.
- [26] RAMSEY, A.T., TURNER, S.L., Rev. Sci. Instrum. **58** (1987) 1211.
- [27] SADLER, G. J., van BELLE, P., in Controlled Fusion and Plasma Physics (Proc. 22nd Eur. Conf. Bournemouth, 1995), Vol. 19C, Part II, European Physical Society, Geneva (1995) 269.
- [28] GORELENKOV, N. N., et al., Nucl. Fusion **37** (1997) 1053.

- [29] GORELENKOV, N. N., PUTVINSKII, S. V., *Sov. J. Plasma Phys.* **15** (1989) 145.
- [30] PUTVINSKII, S. V., *Reviews of Plasma Physics*, Vol. 18, Consultants Bureau, New York (1993) 239.
- [31] YUSHMANOV, P. N., *Nucl. Fusion* **23** (1983) 1599.
- [32] GOLDSTON, R. J., et al., *Phys. Rev. Lett.* **47** (1981) 647.
- [33] PARKS, P. B., *Plasma Phys. Control. Fusion* **38** (1996) 571.
- [34] McKEE, G. R., et al., *Phys. Rev. Lett.* **75** (1995) 649.
- [35] ZWEBEN, S. J., et al., *Nucl. Fusion* **35** (1995) 893.
- [36] KRASILNIKOV, A. V., et al., *Rev. Sci. Instrum.* **68** (1997) 553.
- [37] McKEE, G. R., et al., *Nucl. Fusion* **37** (1997) 501.
- [38] REDI, M. H., et al., *Phys. Plasmas* **4** (1997) (In press).
- [39] WHITE, R. B., et al., *Phys. Plasmas* **3** (1996) 3043.
- [40] REDI, M. H., et al., in *Controlled Fusion and Plasma Physics (Proc. 24th Eur. Conf. Berchtesgaden, 1997)*, Vol. 21C, Part ??, European Physical Society, Geneva (1997) ???.
- [41] DARROW, D. S., et al., *Rev. Sci. Instrum.* **66** (1995) 476.
- [42] KOLESNICHENKO, Ya. I., et al., *Nucl. Fusion* **32** (1992) 449.
- [43] STRATTON, B. C., et al., *Nucl. Fusion* **36** (1996) 1586.
- [44] KOLESNICHENKO, Ya. I., et al., *Nucl. Fusion* **36** (1996) 159.
- [45] KOLESNICHENKO, Ya. I., et al., *Phys. Plasmas* **4** (1997) 2544.
- [46] KADOMTSEV, B. B., *Sov. J. Plasma Phys.* **1** (1976) 389.
- [47] NAZIKIAN, R., et al., *Phys. Rev. Lett.* **78** (1997) 2976.
- [48] WHITE, R.B., BOOZER, A.H., *Phys. Plasma* **2** (1995) 2915.
- [49] MAJESKI, R., et al., *Phys. Plasmas* **3** (1996) 2006.
- [50] POST, D.E., in *Plasma Physics and Controlled Nuclear Fusion Research 1991 (Proc. 13th Int. Conf. Washington, 1990)*, Vol. 3, International Atomic Energy Agency, Vienna (1991) 239.

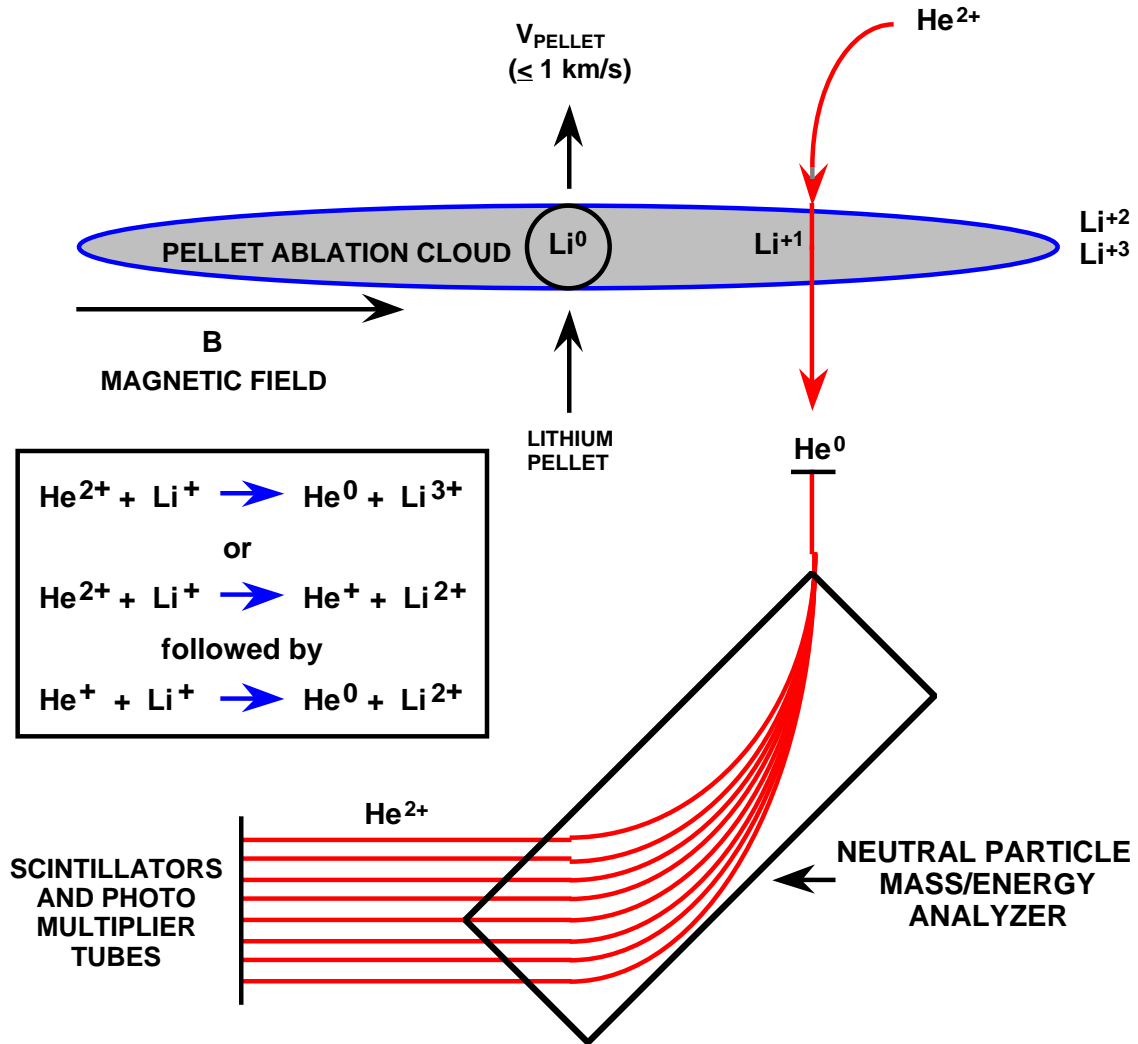


Fig. 1 Illustration of the Pellet Charge eXchange (PCX) concept using lithium as an example of low-Z impurity pellet injection.



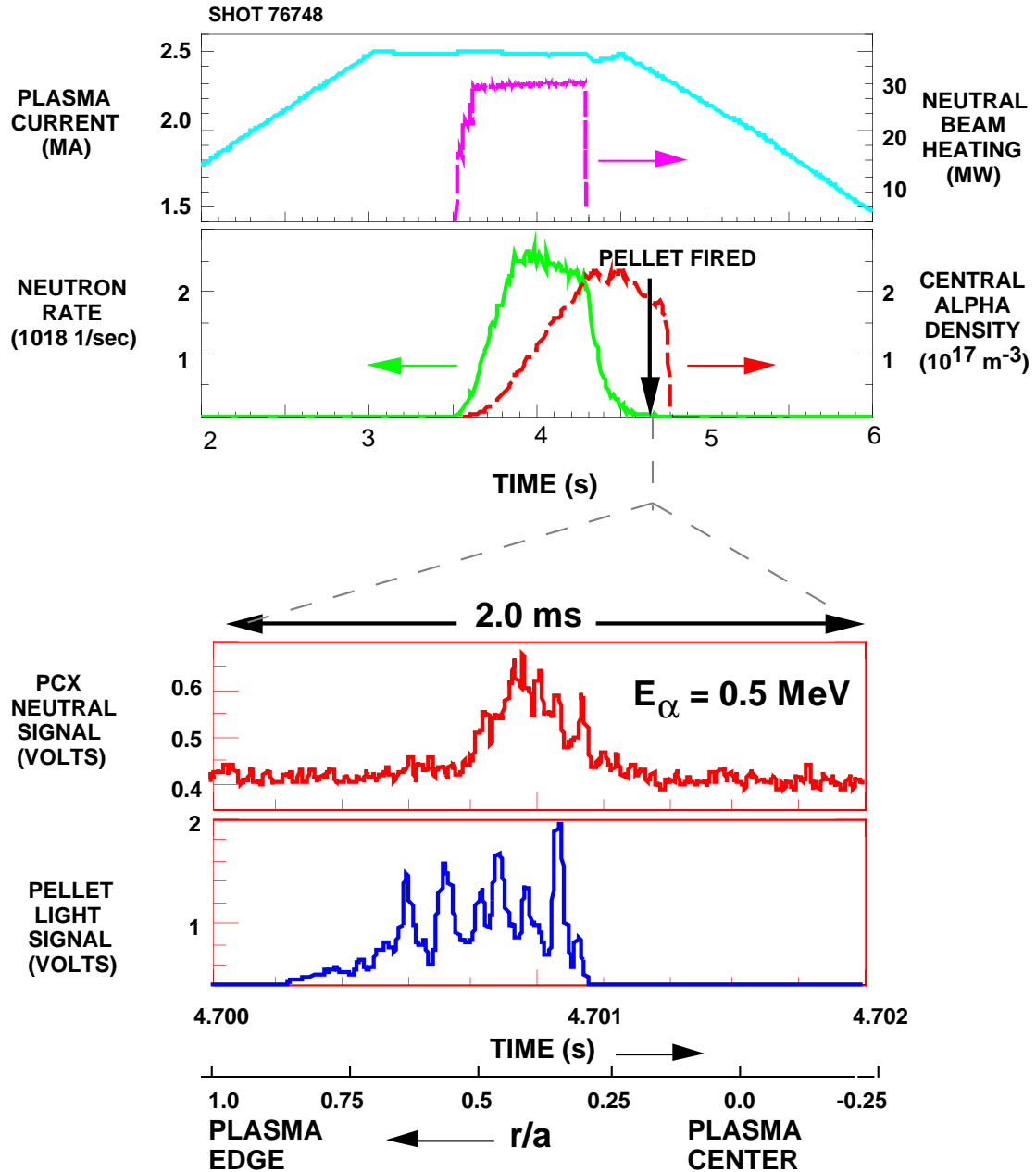


Fig. 2 Selected plasma waveforms (upper panels) and PCX signals (lower panels) illustrating a typical measurement scenario and characteristics of the neutral particle and pellet light signals for the PCX diagnostic. The fluctuations on the neutral signal are due to counting statistics and do not correlate with the fluctuations on the light signal, presumably because the ablation cloud remains an equilibrium thick neutralization target at all times.

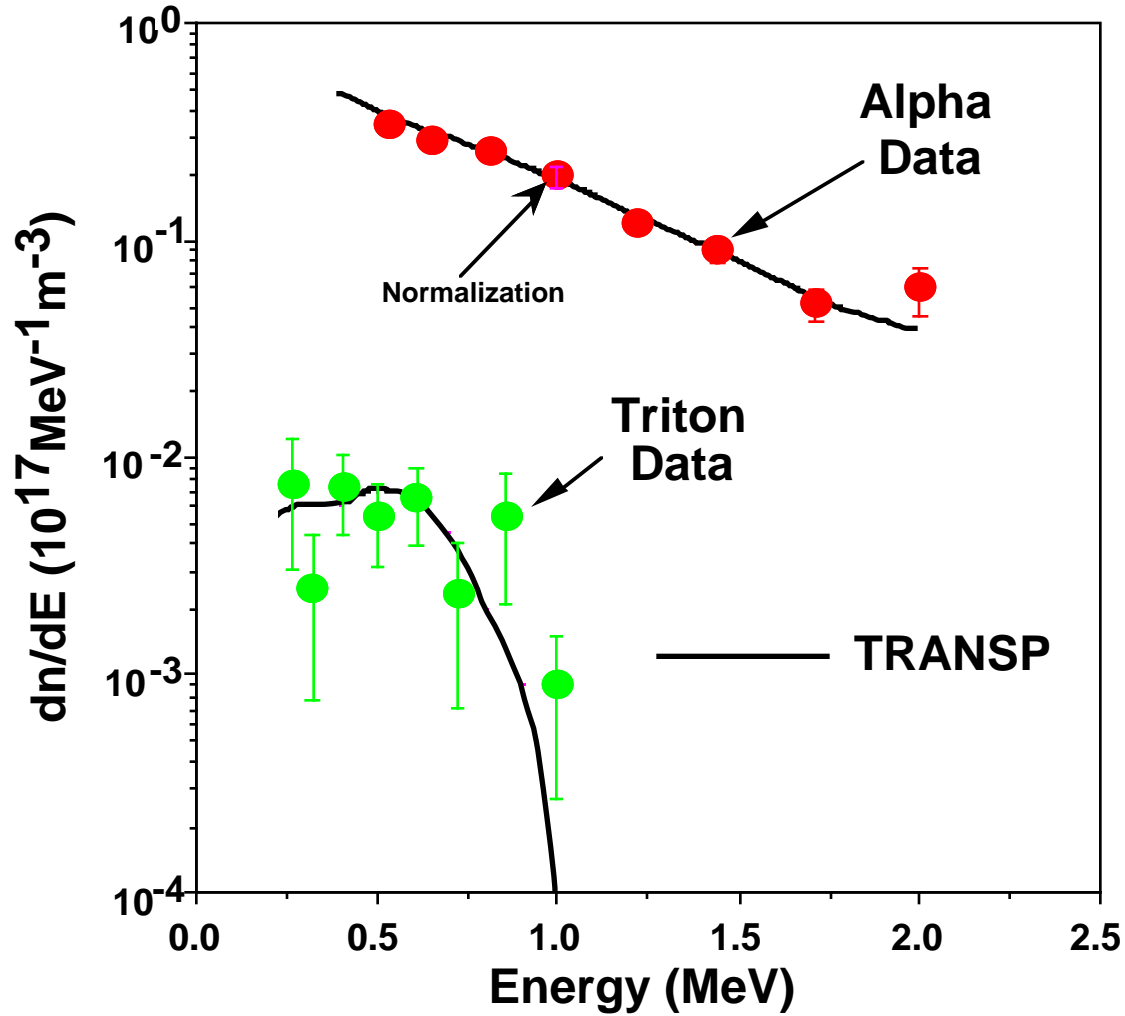


Fig. 3 Comparison of the PCX measurements of the alpha spectrum from an MHD-quietest D-T discharge (#78706) and the triton spectrum from a similar D-D discharge (#78601) with TRANSP predictions. Both the shape of the energy spectra and the alpha-to-triton ratio agree well with the TRANSP simulations, which assume classical alpha thermalization.

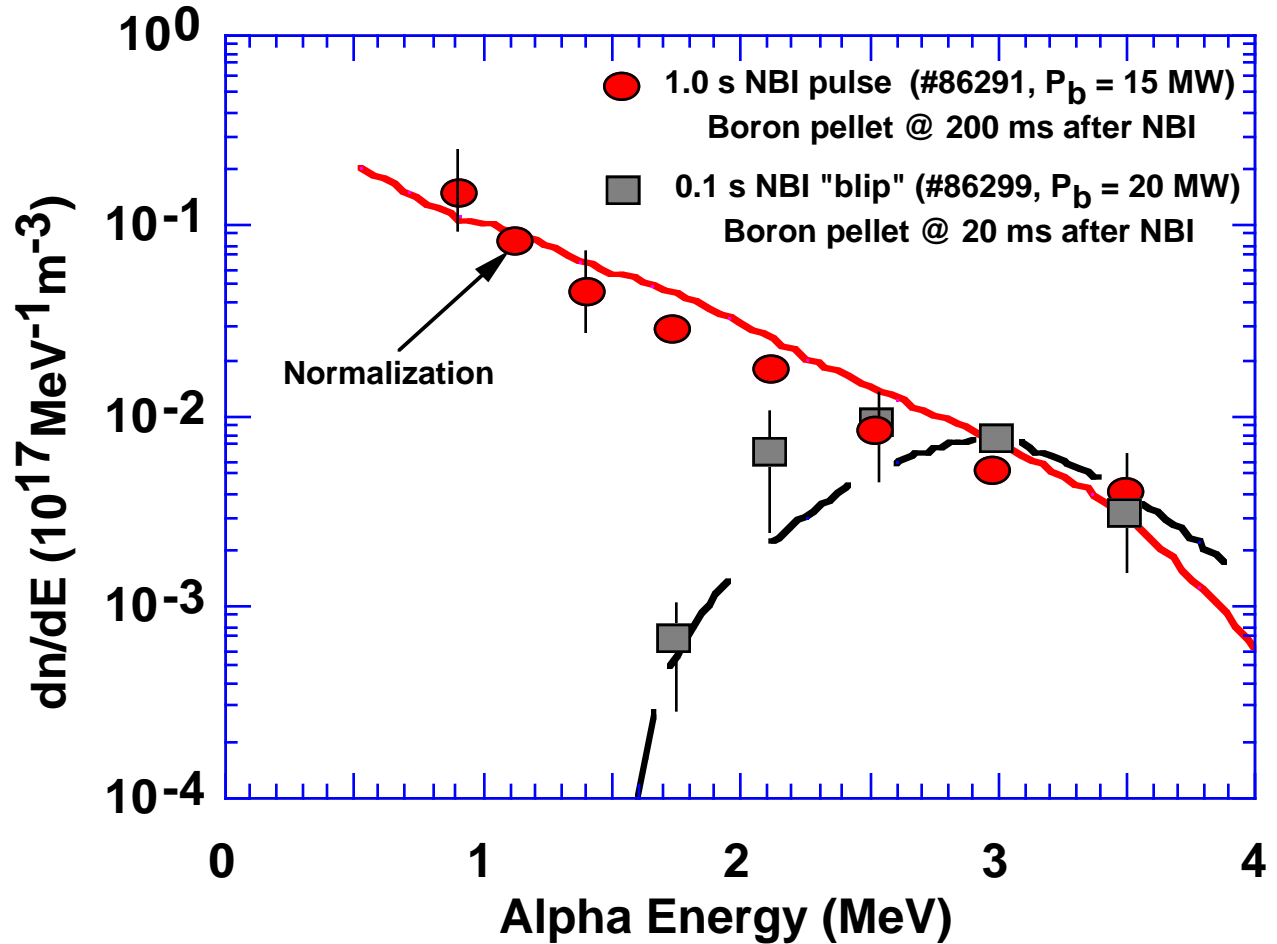


Fig. 4 Comparison of measured alpha energy spectra with FPPT simulation during the fully slowed down phase (circles and solid curve) and partially slowed down phase (squares and dashed curve). The agreement indicates that alpha particles thermalize classically in the core of MHD-quiescent supershot discharges.

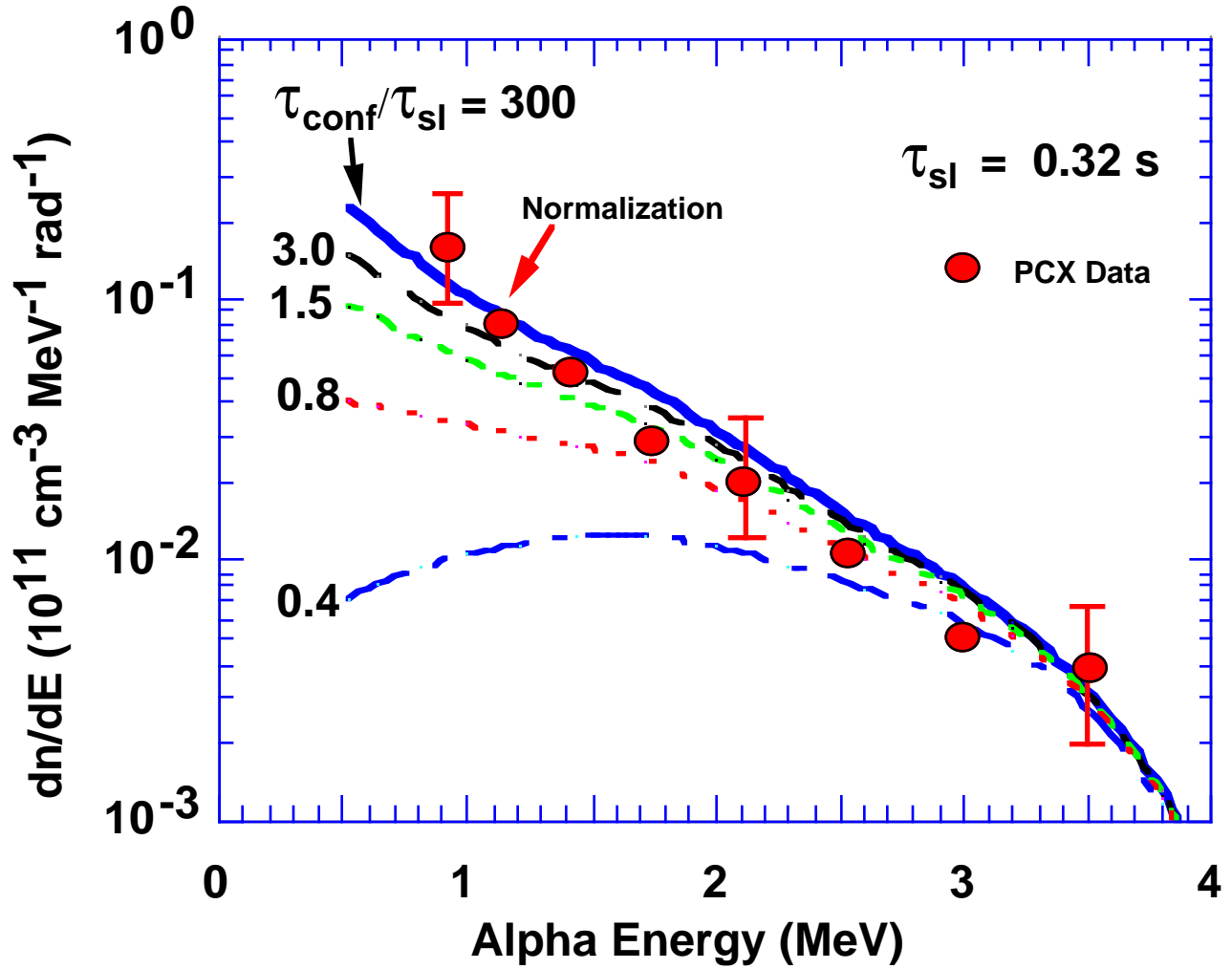


Fig. 5 In comparison with the FPPT simulation, the PCX alpha slowing down spectrum is consistent with an alpha confinement time of  $\tau_{\text{conf}} > 3.0 \tau_{\text{sl}}$ .

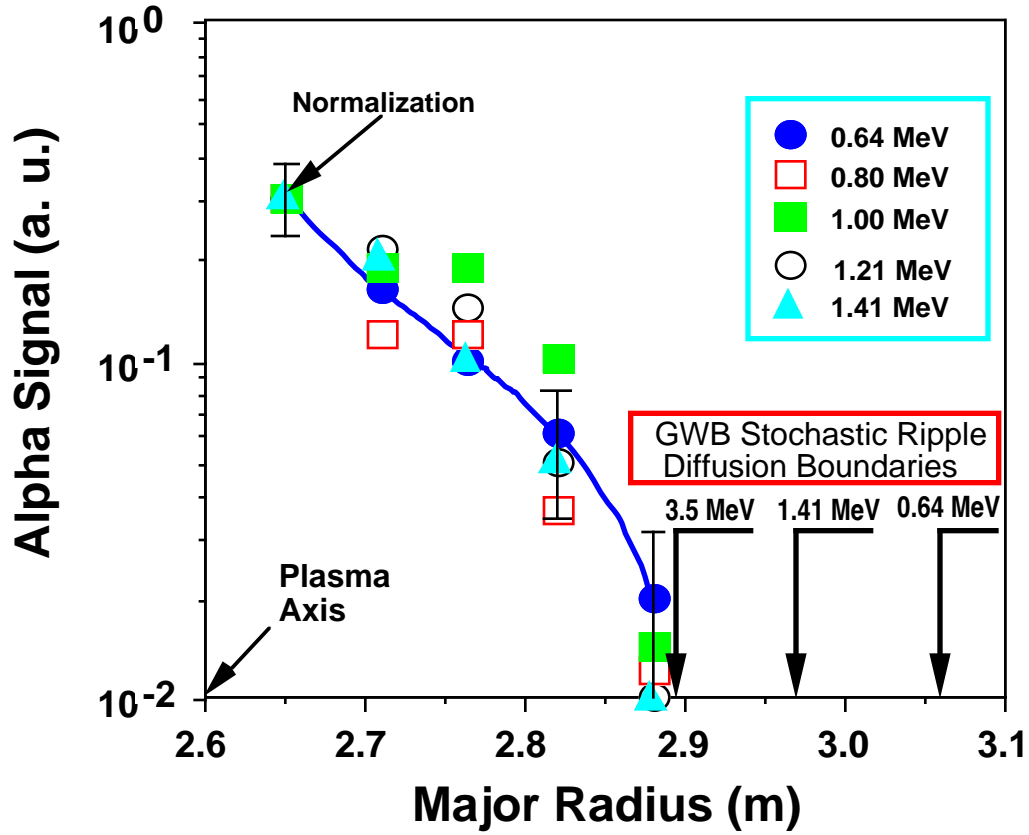


Fig. 6 In a sawtooth free discharge (#84550), the measured radial profiles of the alpha signal are similar for all energies and are delimited by the stochastic ripple loss boundary for  $E_\alpha = 3.5$  MeV. The solid curve shows the FPPT profile simulation for  $E_\alpha = 1.0$  MeV.

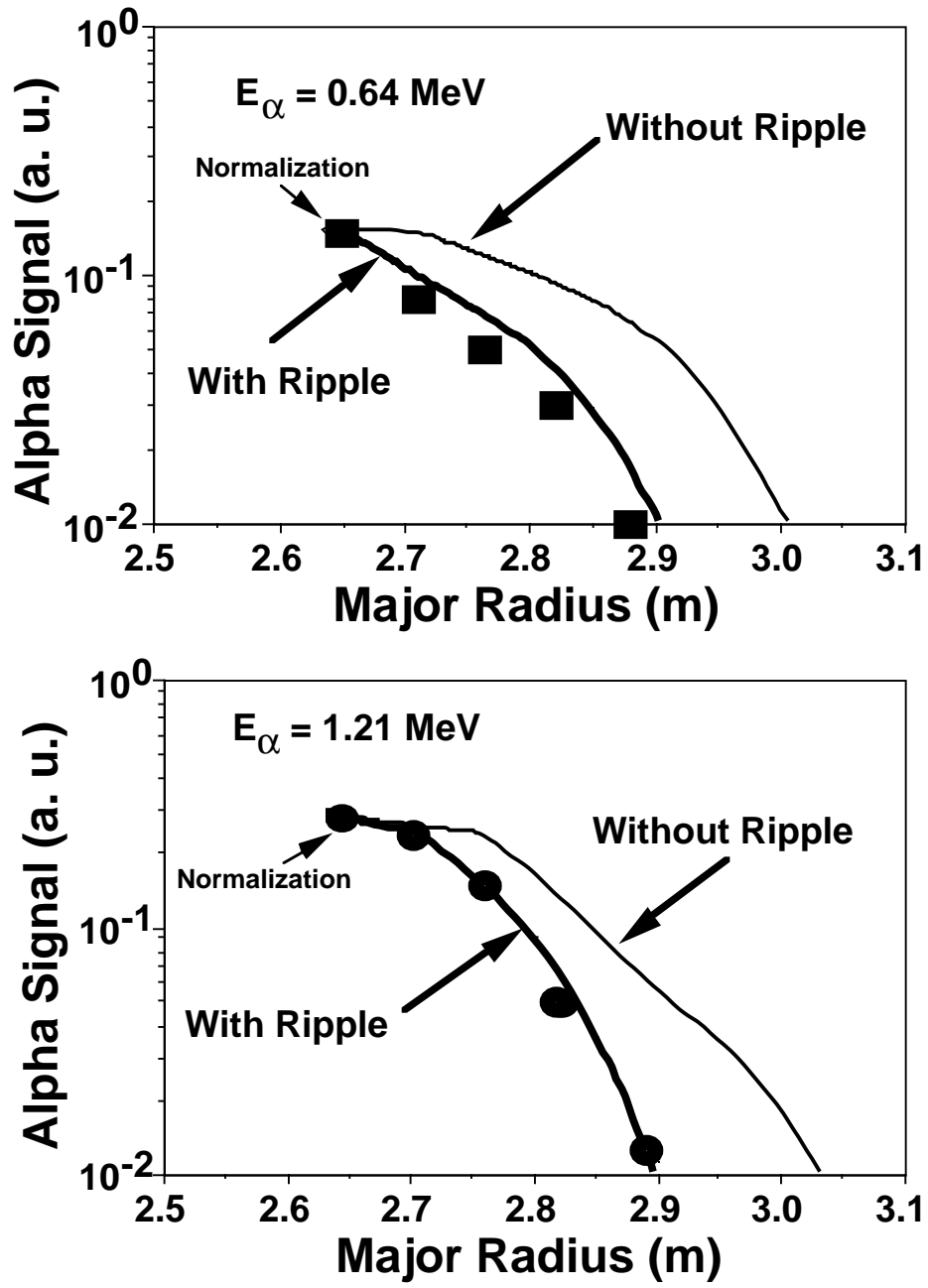


Fig. 7 The PCX measured radial profiles of the alpha signal in a sawtooth-free discharge (#84550) agree well with FPPT modeling which includes stochastic ripple diffusion.

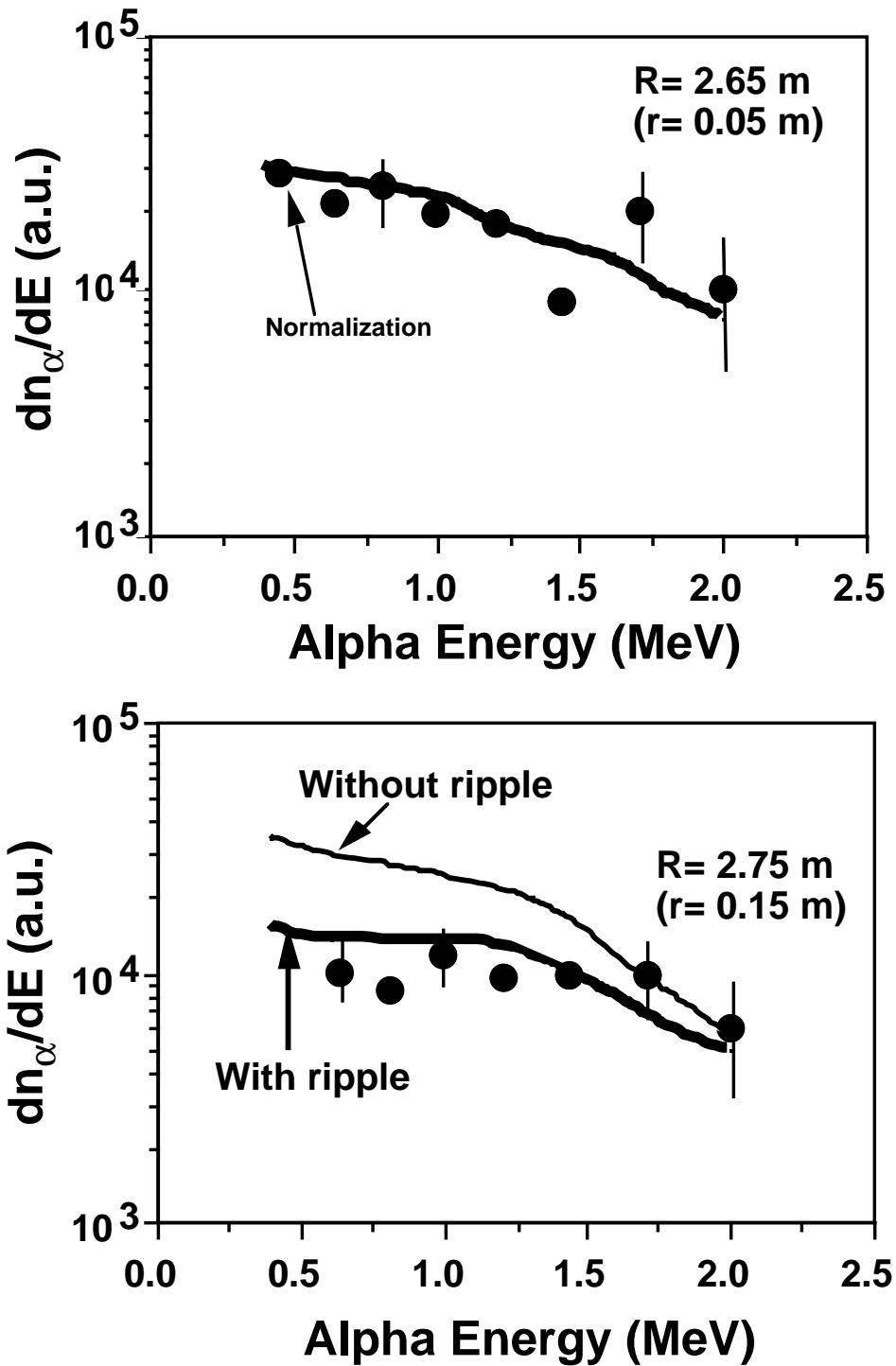


Fig. 8 The PCX measured alpha energy spectra in a sawtooth-free discharge (#84550) agree with stochastic ripple diffusion modeling in the FPPT code. In the ripple-free plasma core (top panel), the simulation with and without ripple is the same.

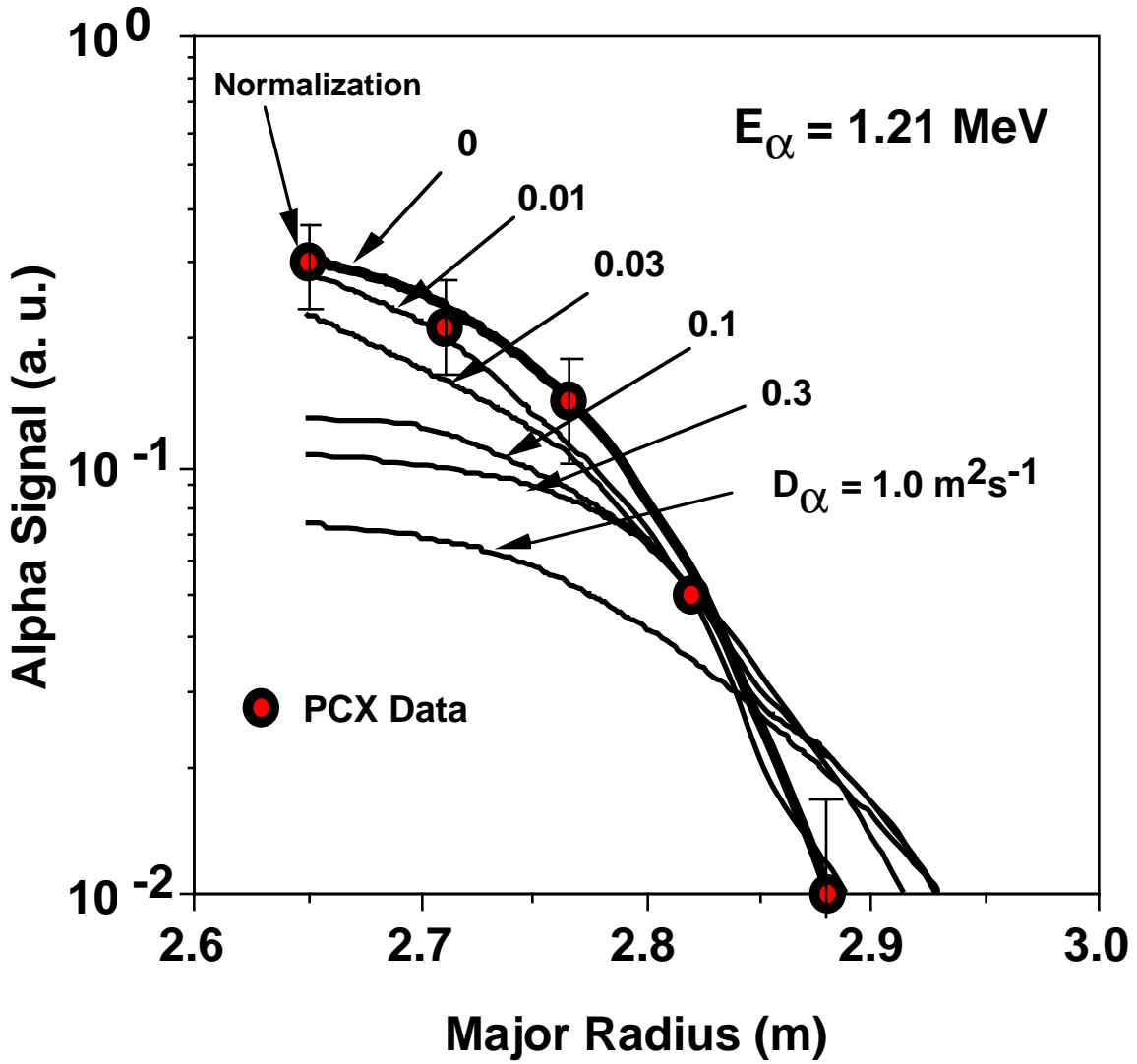


Fig. 9 In comparison with the FPPT simulation, the PCX radial profiles of the alpha signal are consistent with a diffusion rate of  $D_\alpha < 0.01 \text{ m}^2\text{s}^{-1}$ .



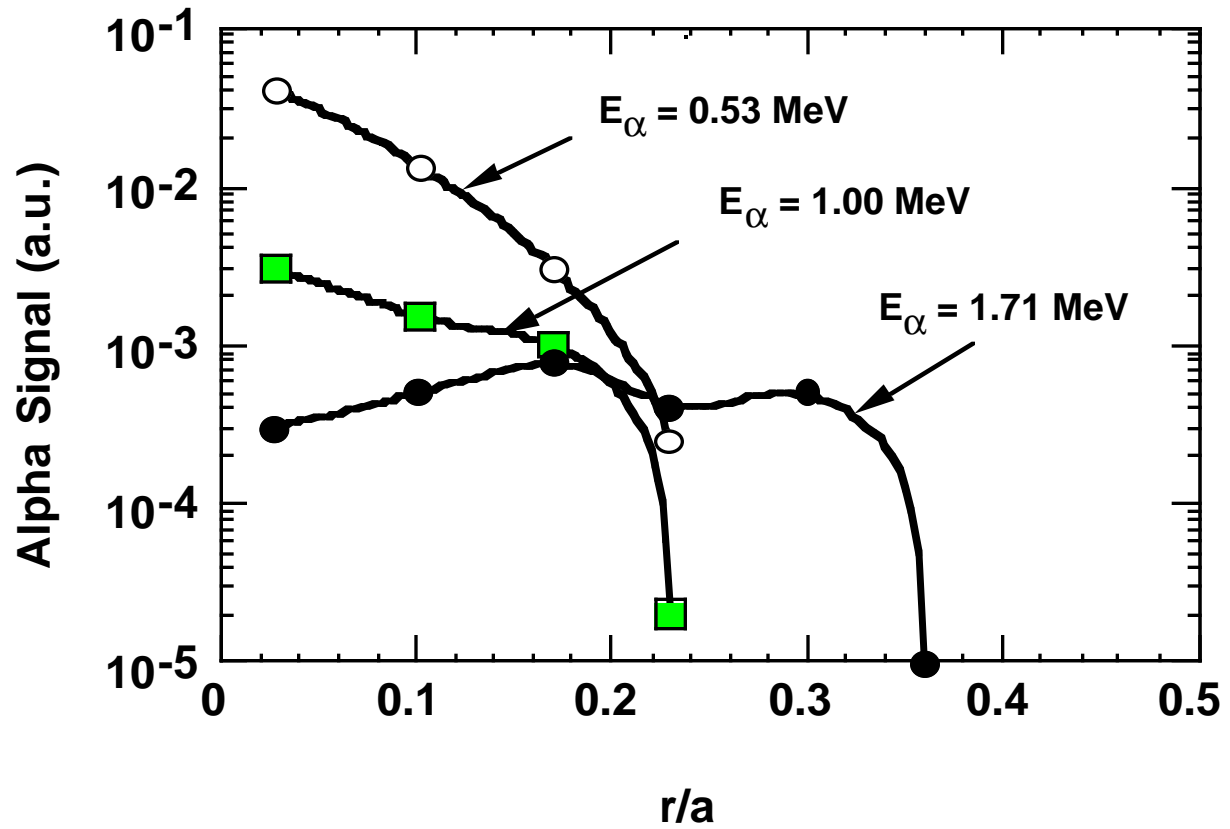


Fig. 10 Redistribution of trapped alpha particles is observed in reversed shear discharges in which the plasma core region is characterized by an elevated  $q$ -factor,  $q(0) \sim 4$ , and strong magnetic shear. Depletion of alpha particles in the core and profile broadening appear to increase with increasing alpha energy.

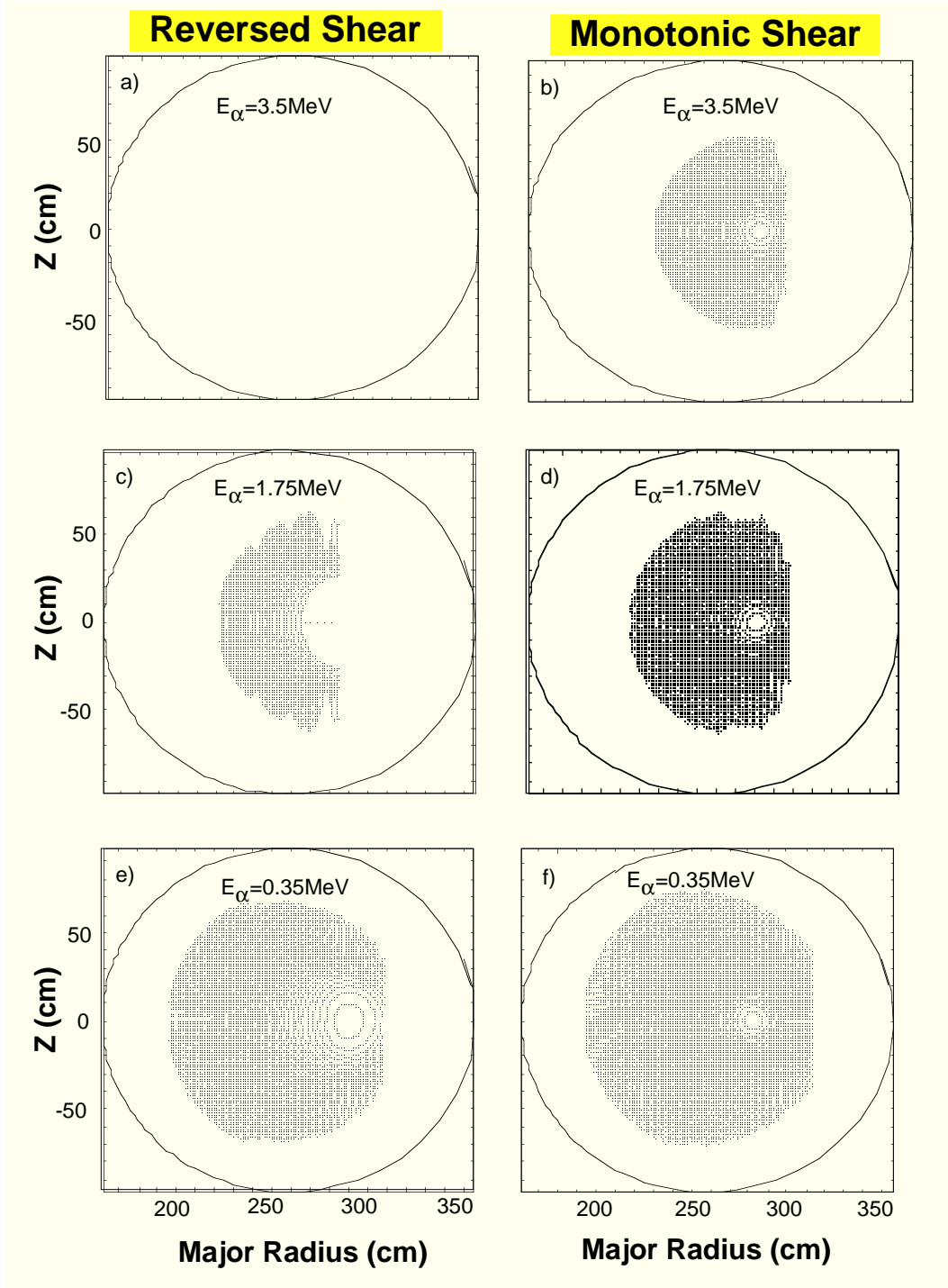


Fig. 11 Shown are ORBIT code calculations of the alpha banana tip confinement domains (hatched regions) for monotonic and reversed shear scenarios for  $E_\alpha = 0.35, 1.75,$  and  $3.5 \text{ MeV}$ . In reversed shear discharges, all alphas born on trapped orbits are rapidly lost.

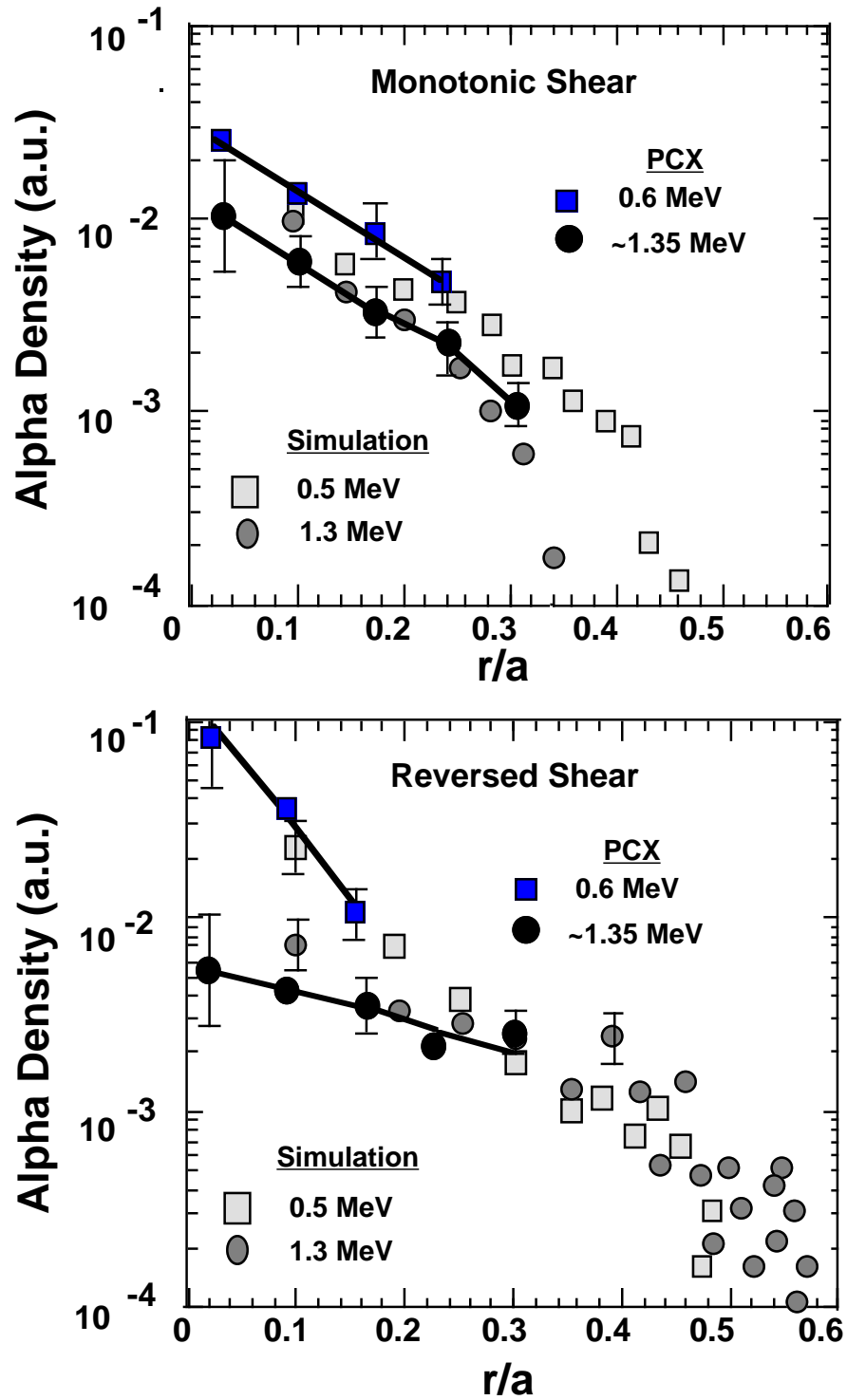


Fig. 12 Agreement between the radial profiles of the alpha signal from PCX measurements and the ORBIT simulations is seen for both monotonic and reversed shear scenarios, including the energy dependence of the profiles in the reversed shear case.

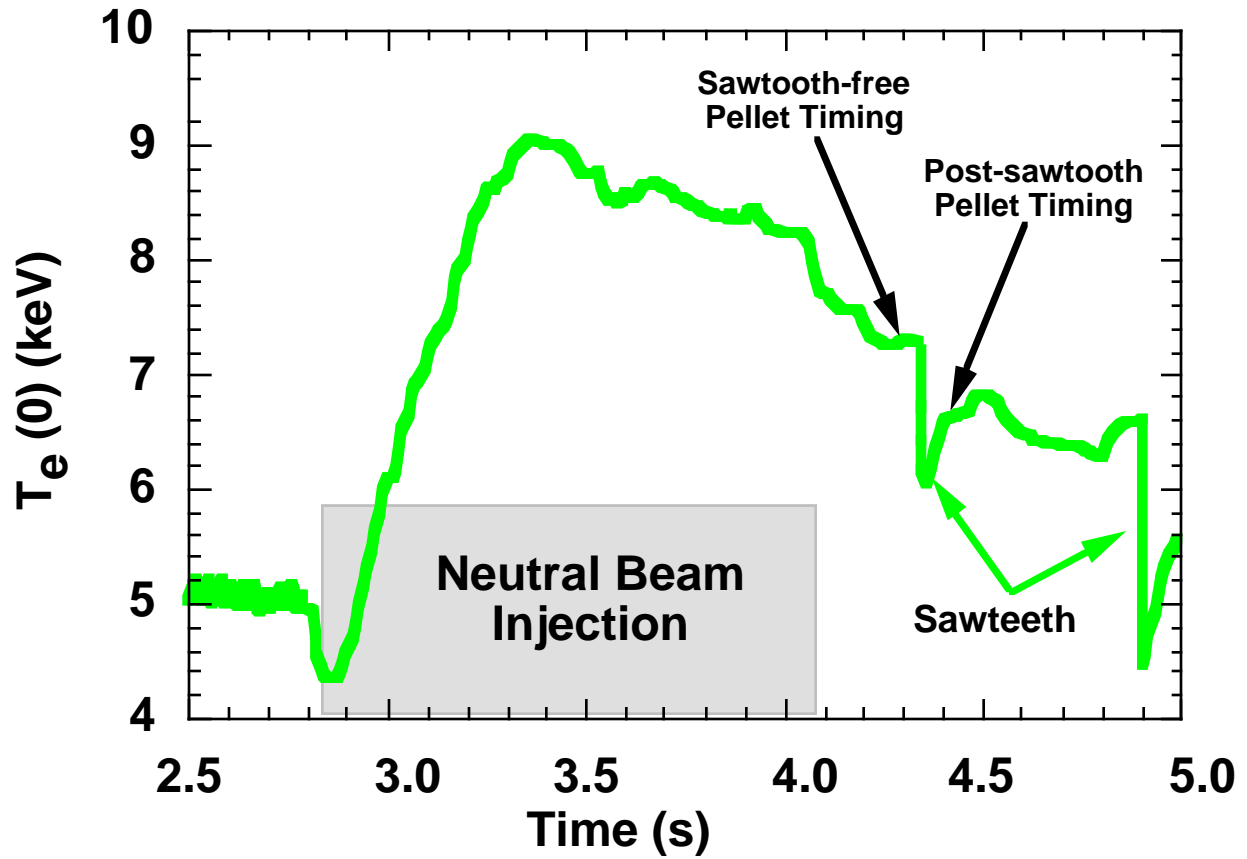


Fig. 13 In TFTR supershots, sawtooth activity typically begins  $0.25 \pm 0.5$  s after termination of beam injection. For PCX measurements, post-NBI timing enhances both pellet penetration (due to the decay of  $T_e$  and  $n_e$ ) and the signal-to-noise ratio (because the neutron emission decays faster than the energetic ion density).

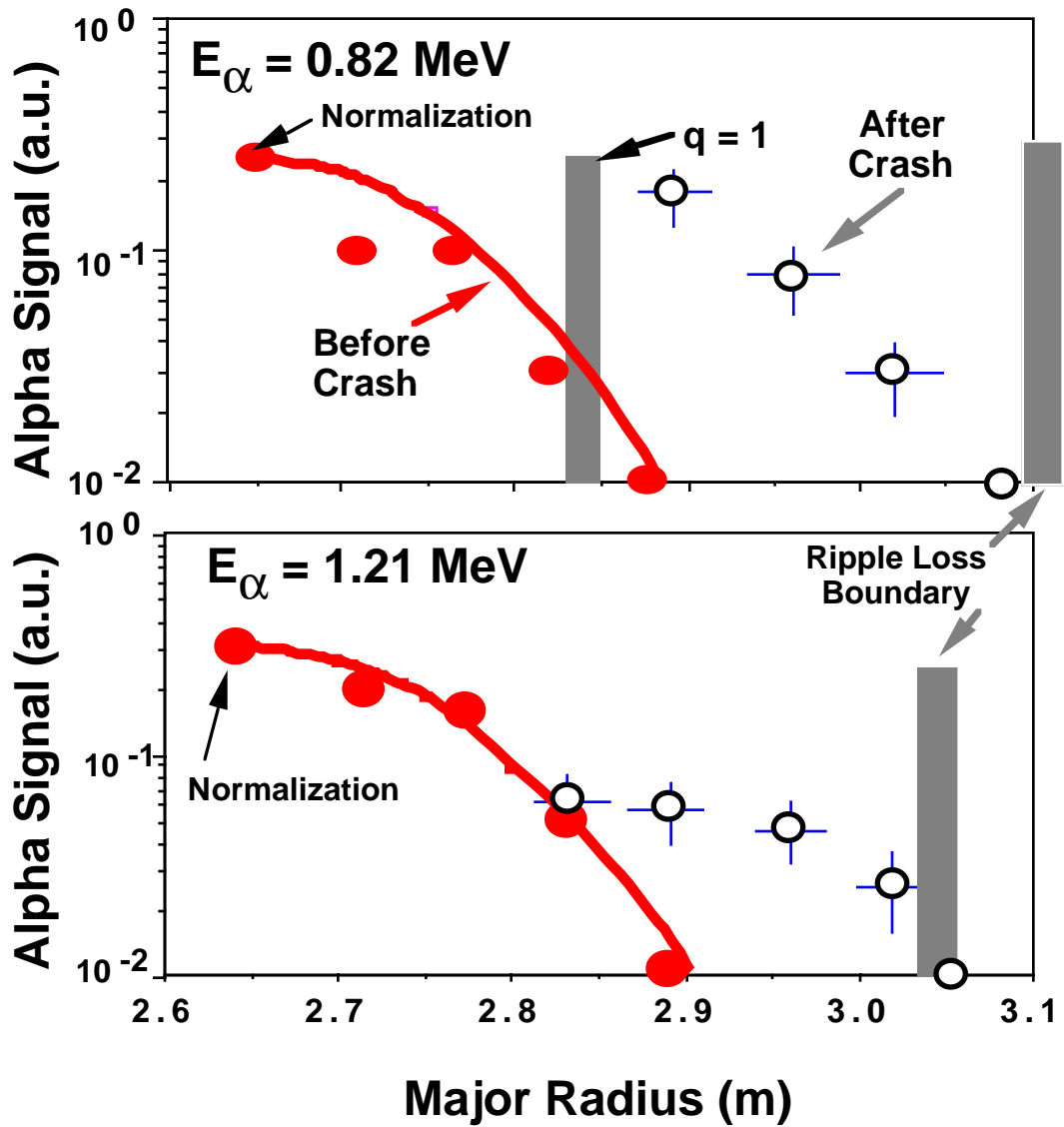


Fig. 14 In the presence of strong sawtooth activity, alphas are depleted in the core and redistributed to well outside the  $q = 1$  radius, but are not observed beyond the stochastic ripple boundary for the associated energy. The observed broadening decreases with increasing energy.

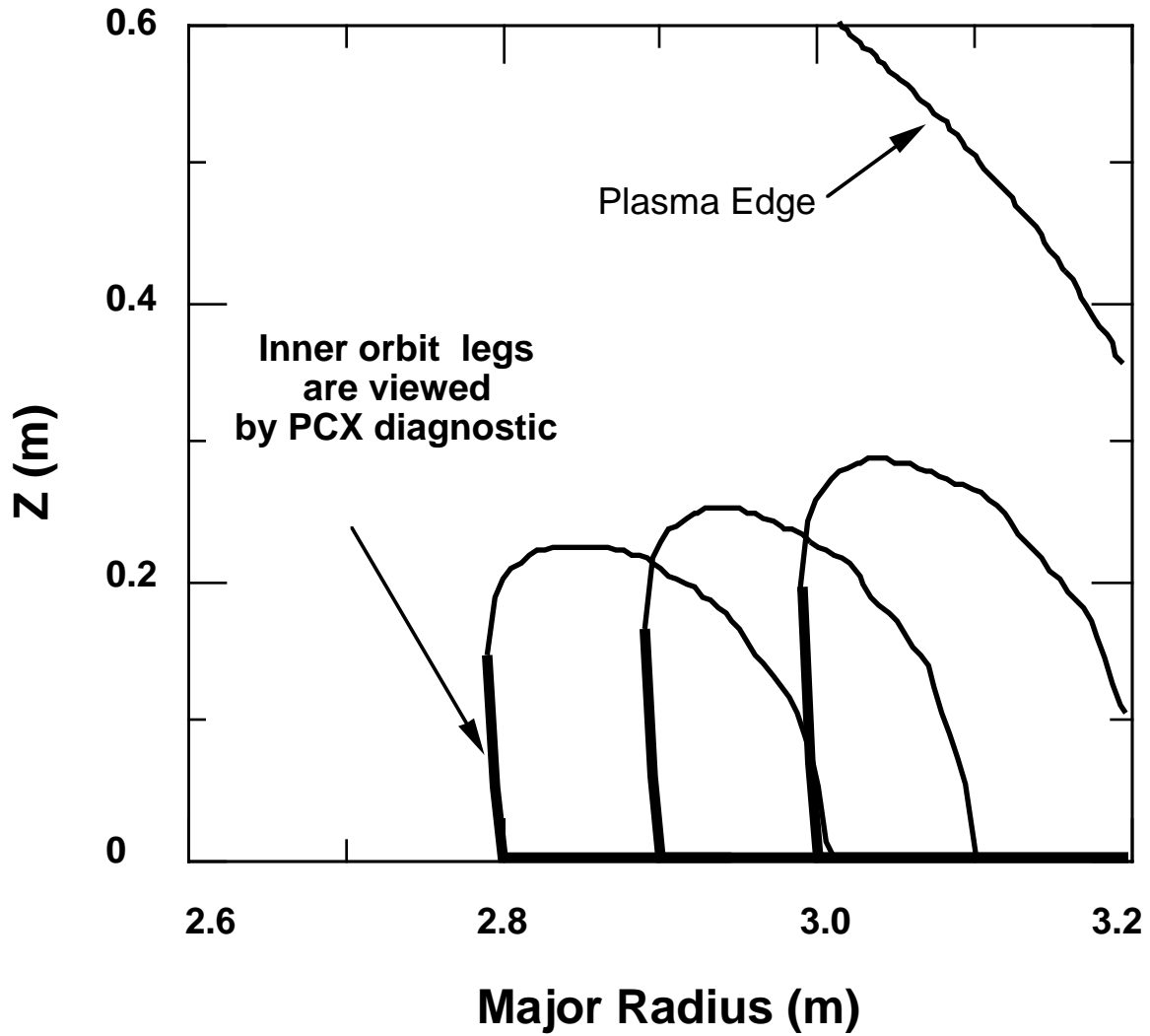


Fig. 15 Illustration of trapped alpha particle orbits for magnetic reconnection modeling. The strong alpha displacement along the major radius, as required to simulate the PCX measurements of alpha sawtooth redistribution, is due to  $E \times B$  drift.

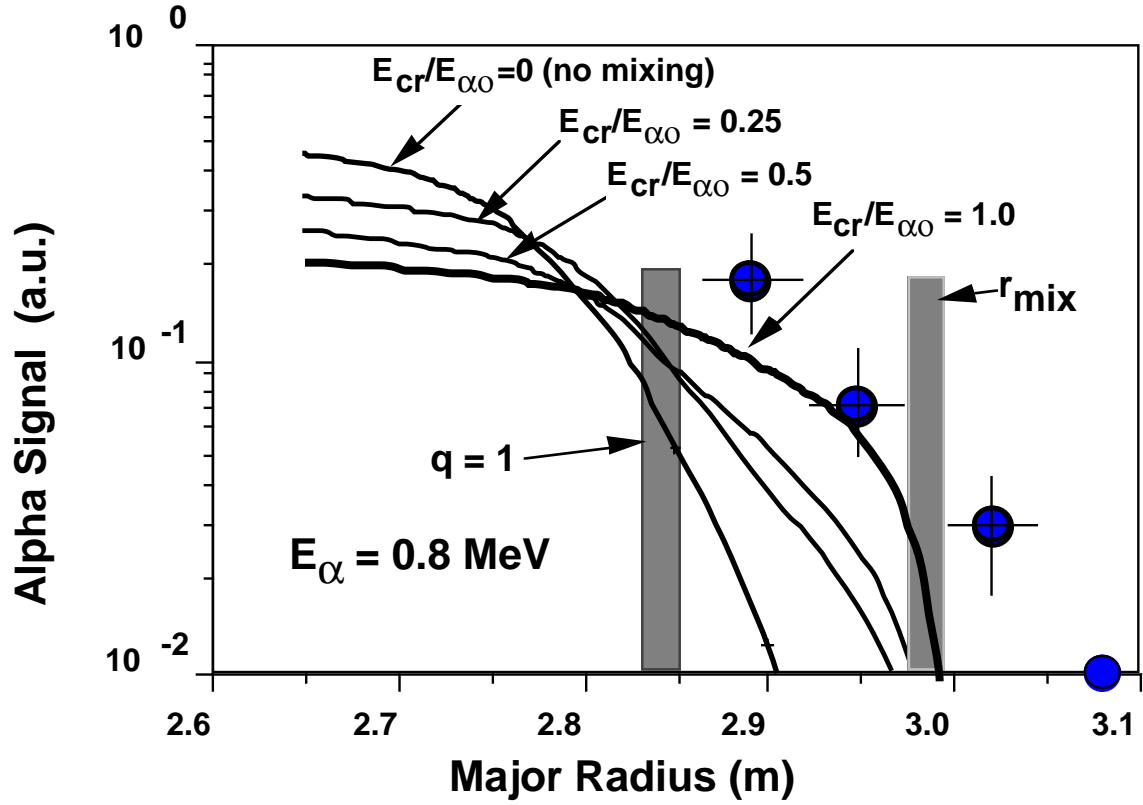


Fig. 16 Selection of the  $E_{cr}$  value for the sawtooth mixing model is illustrated. A value of  $E_{cr} = 3.5 \text{ MeV}$  affords the best fit of the model to the post-sawtooth radial distribution. For this case,  $r_{mix} = 1.5 r_s$ , where  $r_s$  corresponds to the  $n_e$  and  $T_e$  mixing radius at the  $q=1$  surface.

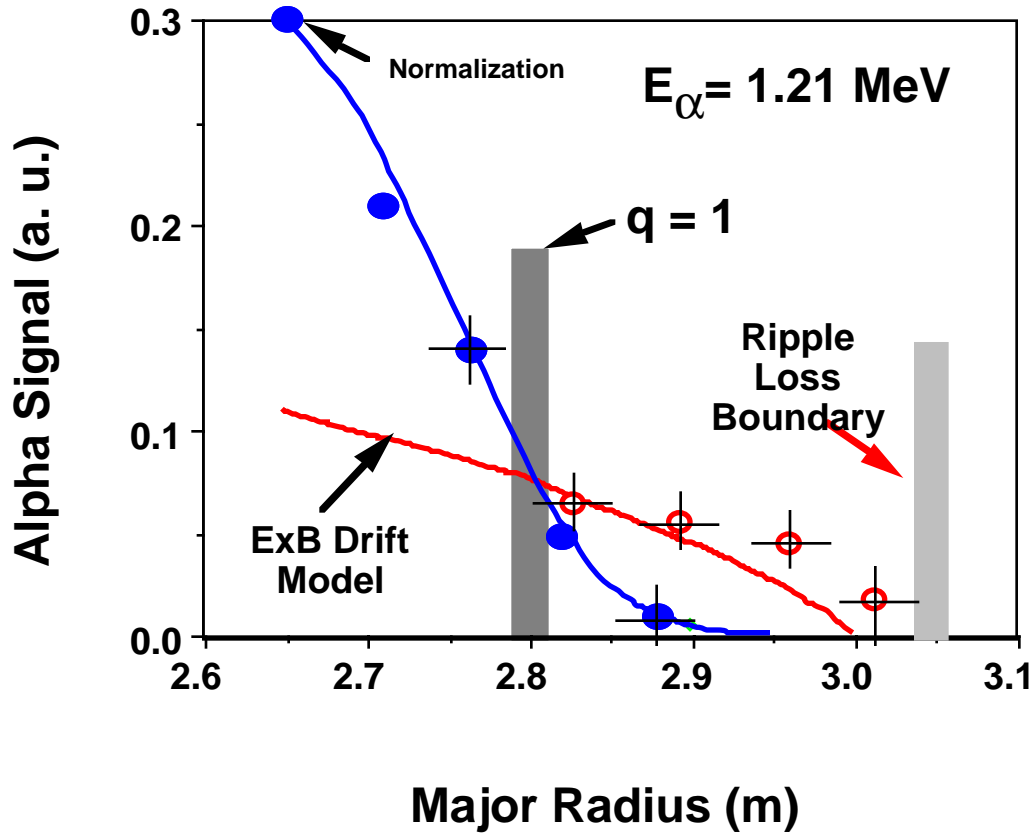


Fig. 17 FPPT simulation of pre-sawtooth radial profile (solid circles - #84550) and post-sawtooth redistribution (open circles - #84549). Reasonable agreement is seen between the PCX sawtooth redistribution measurements and the model.



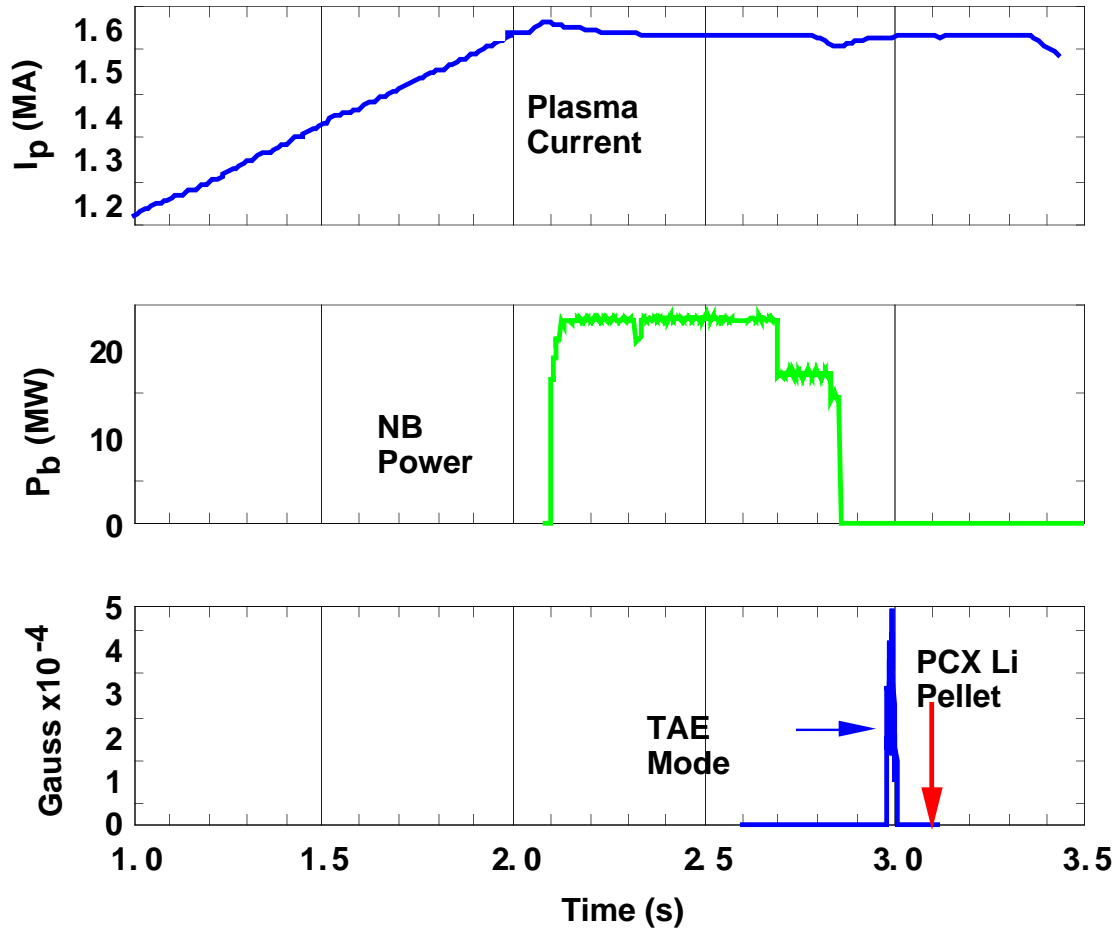


Fig. 18 Scenario for PCX measurement of alpha distributions in the presence of TAE activity. TAE activity typically occurred  $\sim 150$  ms after termination of beam injection. The PCX measurements were performed at post-TAE times in the range of  $\sim 100 \pm 50$  ms.

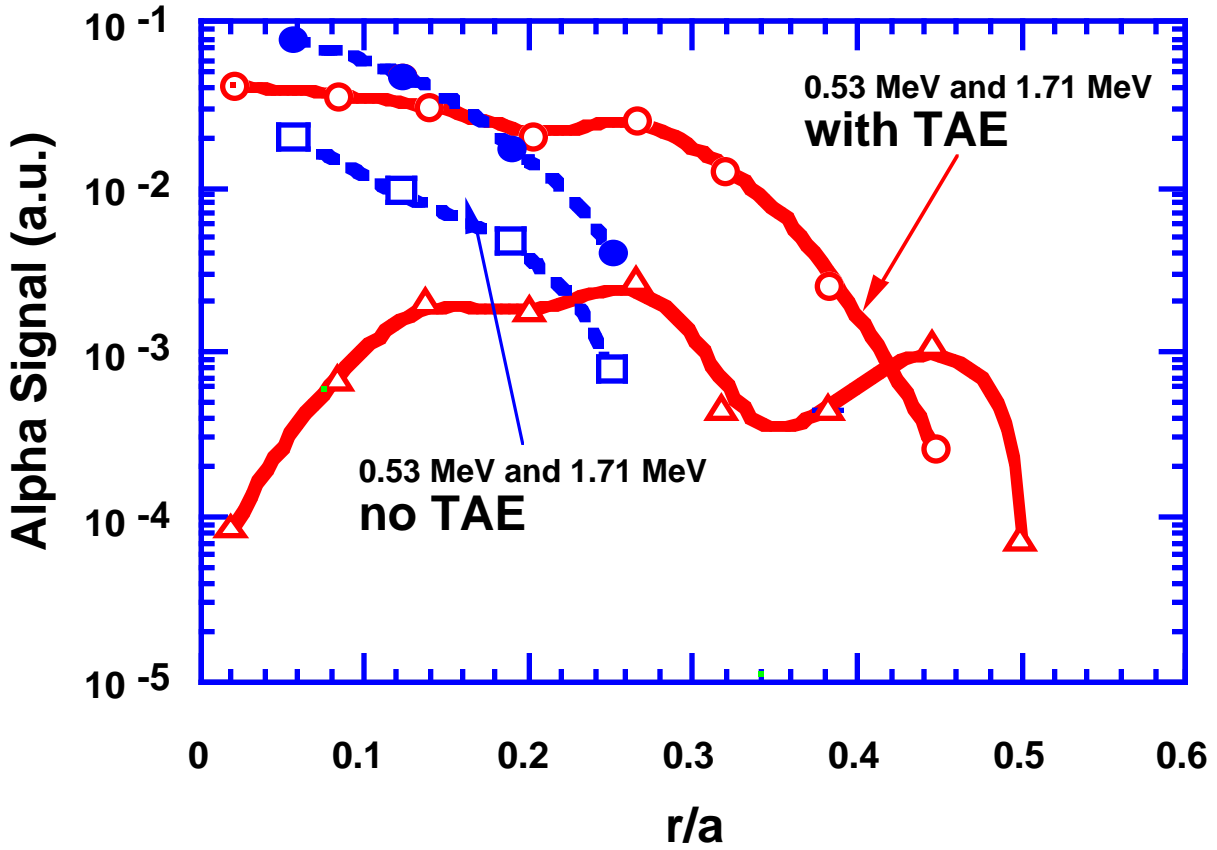


Fig. 19 Redistribution of trapped alpha particles is observed in the presence of TAE modes which have very weak fluctuation levels  $\text{dB/B} \sim 10^{-5}$  in the core. The redistribution becomes broader and more depleted in the core with increasing alpha energy. Significant redistribution occurs only in conjunction with an elevated central q-factor:  $q(0) \sim 2$ .

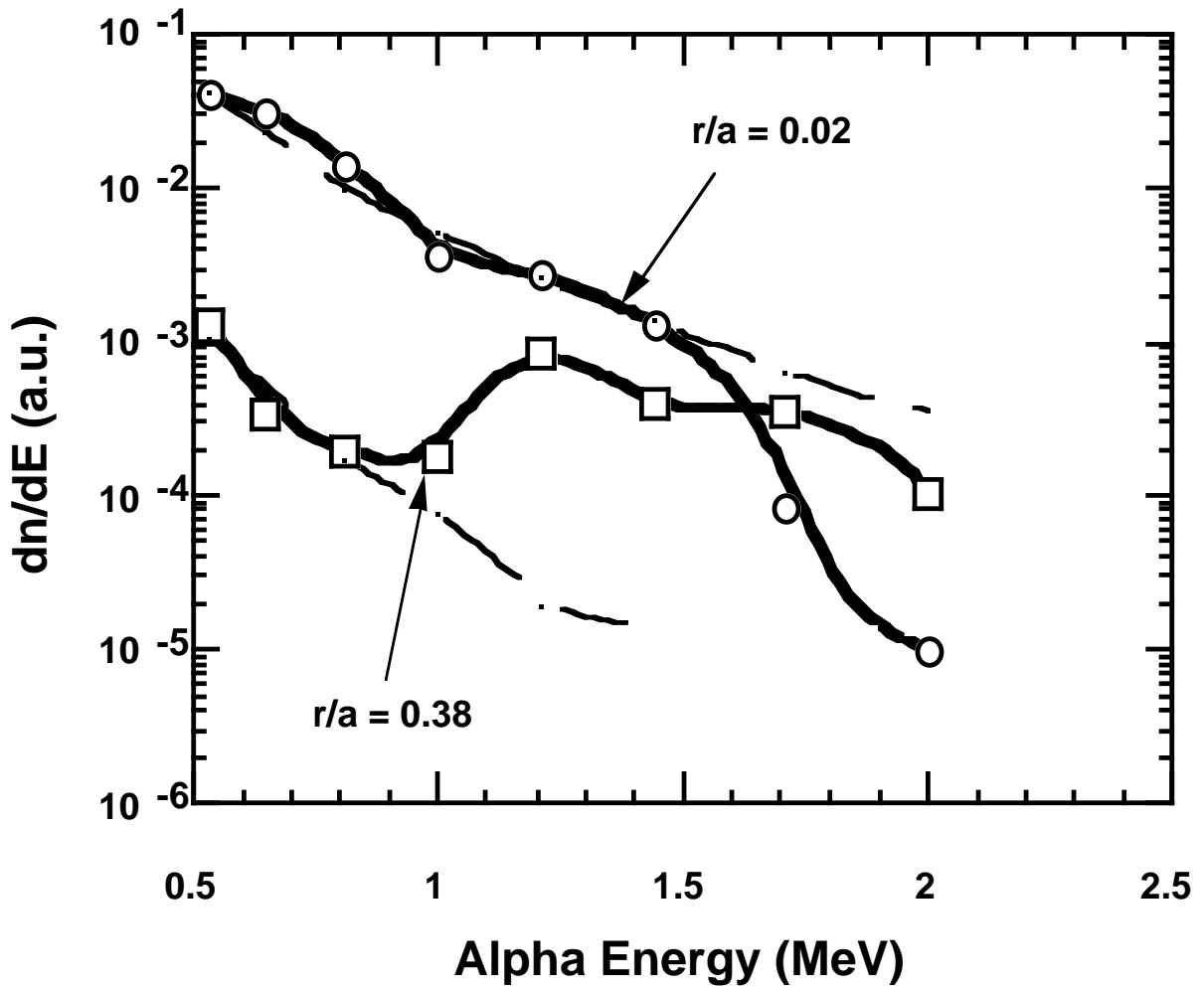


Fig. 20 Alpha particle energy spectra in the presence of TAE models are distorted compared with classical predictions.

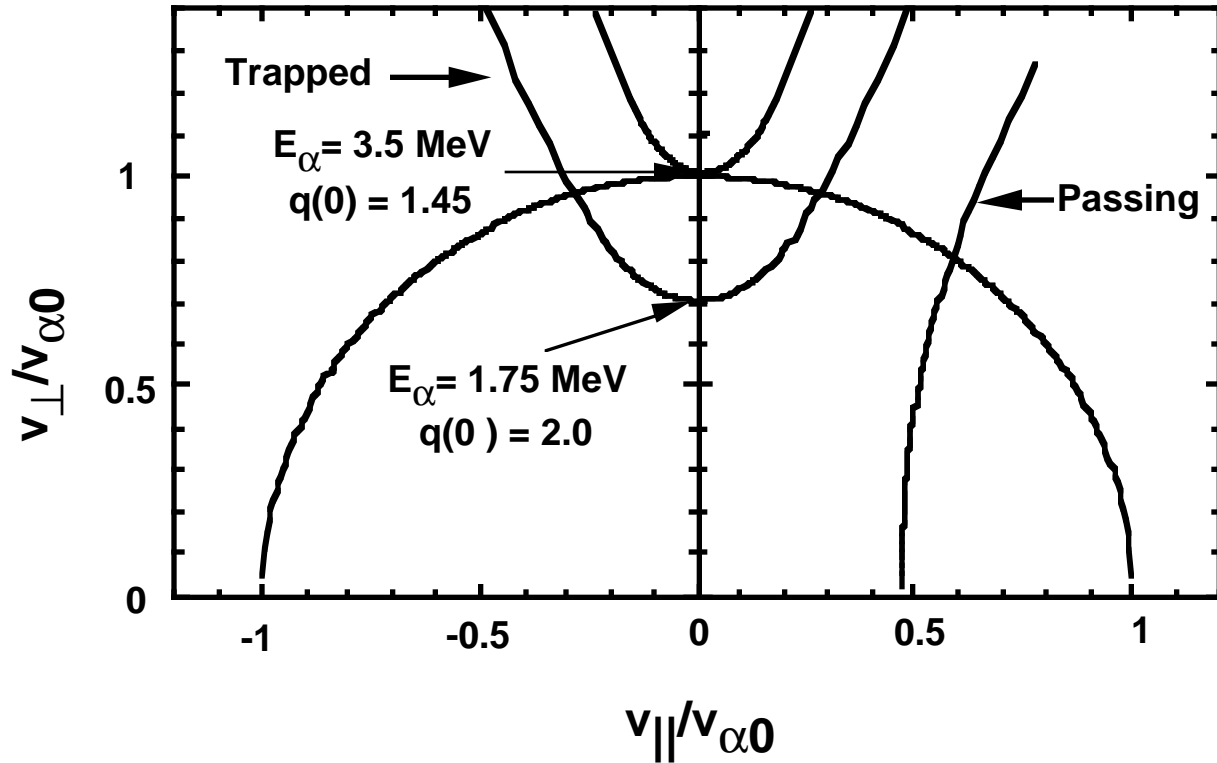


Fig. 21 Illustration of the  $\alpha$ -TAE resonance condition for a representative TFTR discharge scenario. The semi circle is the velocity space boundary for 3.5 MeV alphas while the parabolic-like curves show the resonance condition for the noted alpha energies and safety factors. Lower  $q(0)$  leads to resonances at higher alpha energies. For  $q(0) < 1.45$ , the resonance no longer intersects the alpha distribution.

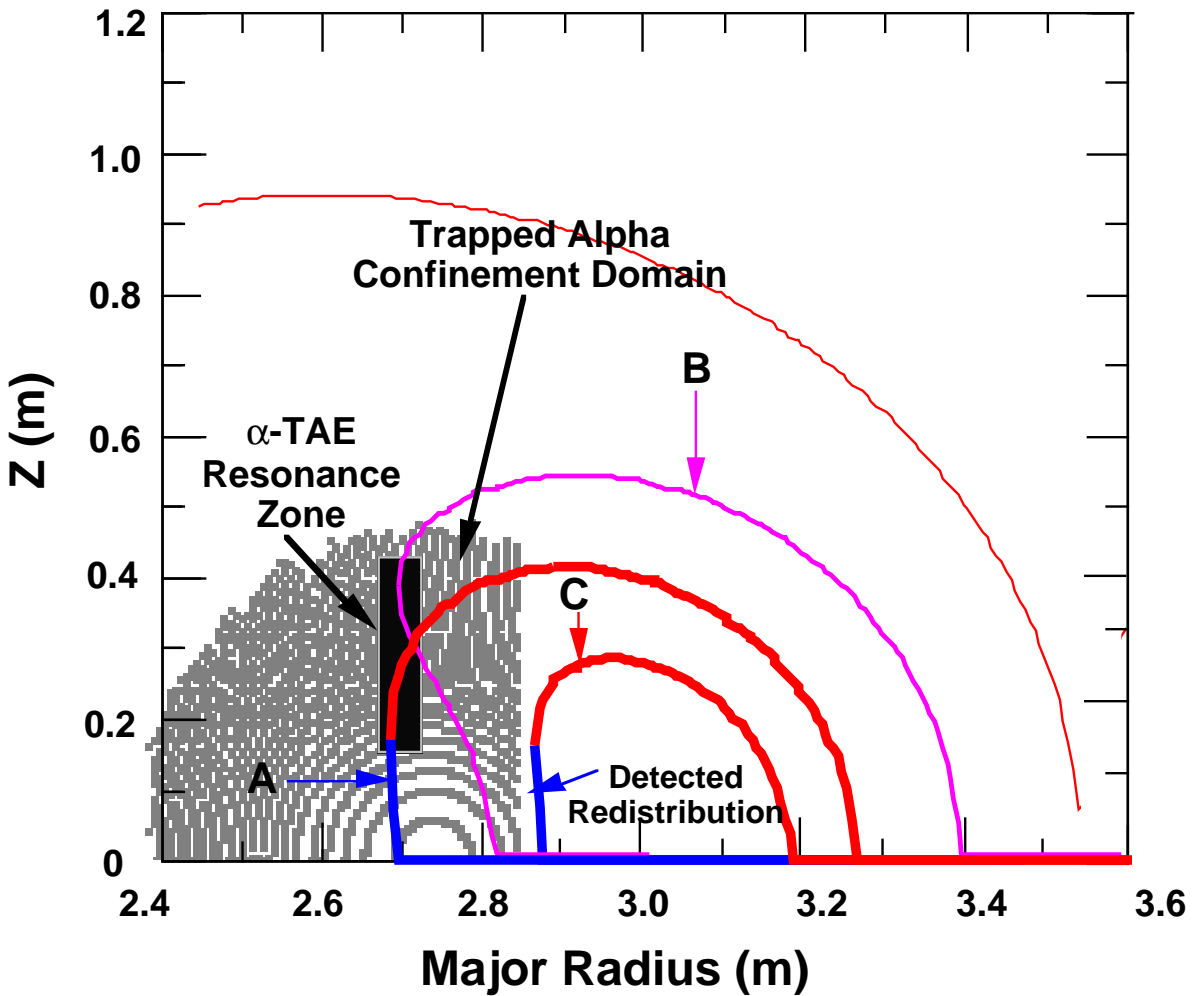


Fig. 22 Illustration of the effect on an initial alpha orbit (A) caused by alpha interaction with the  $\alpha$ -TAE resonance zone shown embedded in the trapped alpha confinement domain. Orbit (B) is produced and subsequent slowing down and pitch angle scattering yields (C). The bolded inner legs indicate orbits for which the alpha pitch angle lies within range viewed by the PCX diagnostic. This proposed process can lead to the alpha redistribution observed by the PCX diagnostic.

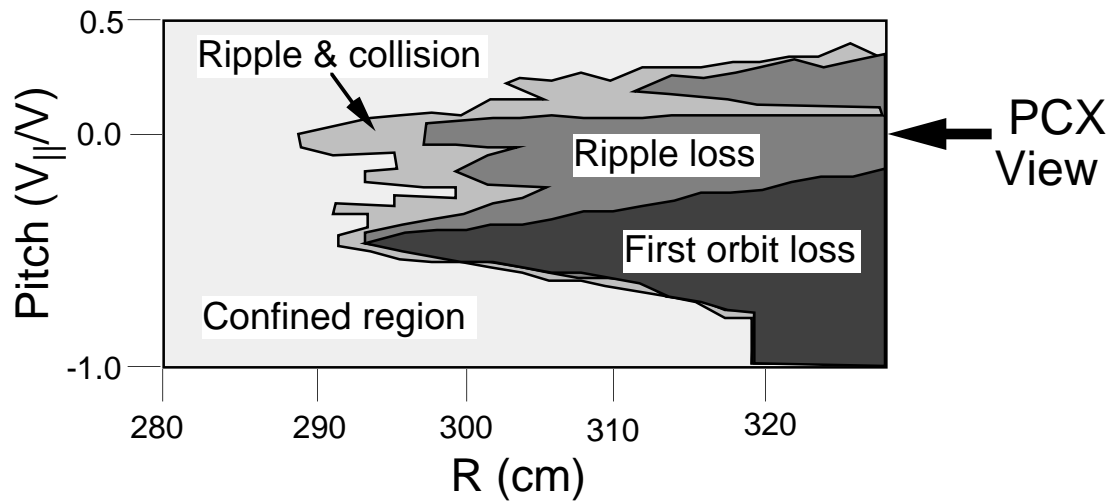


Fig. 23 Map of the alpha loss boundaries in pitch angle and major radius space for the 3.5 MeV alpha particle. The map is created using a Hamiltonian orbit code that follows the alpha guiding center in the rippled plasma equilibrium for an equivalent slowing down time.

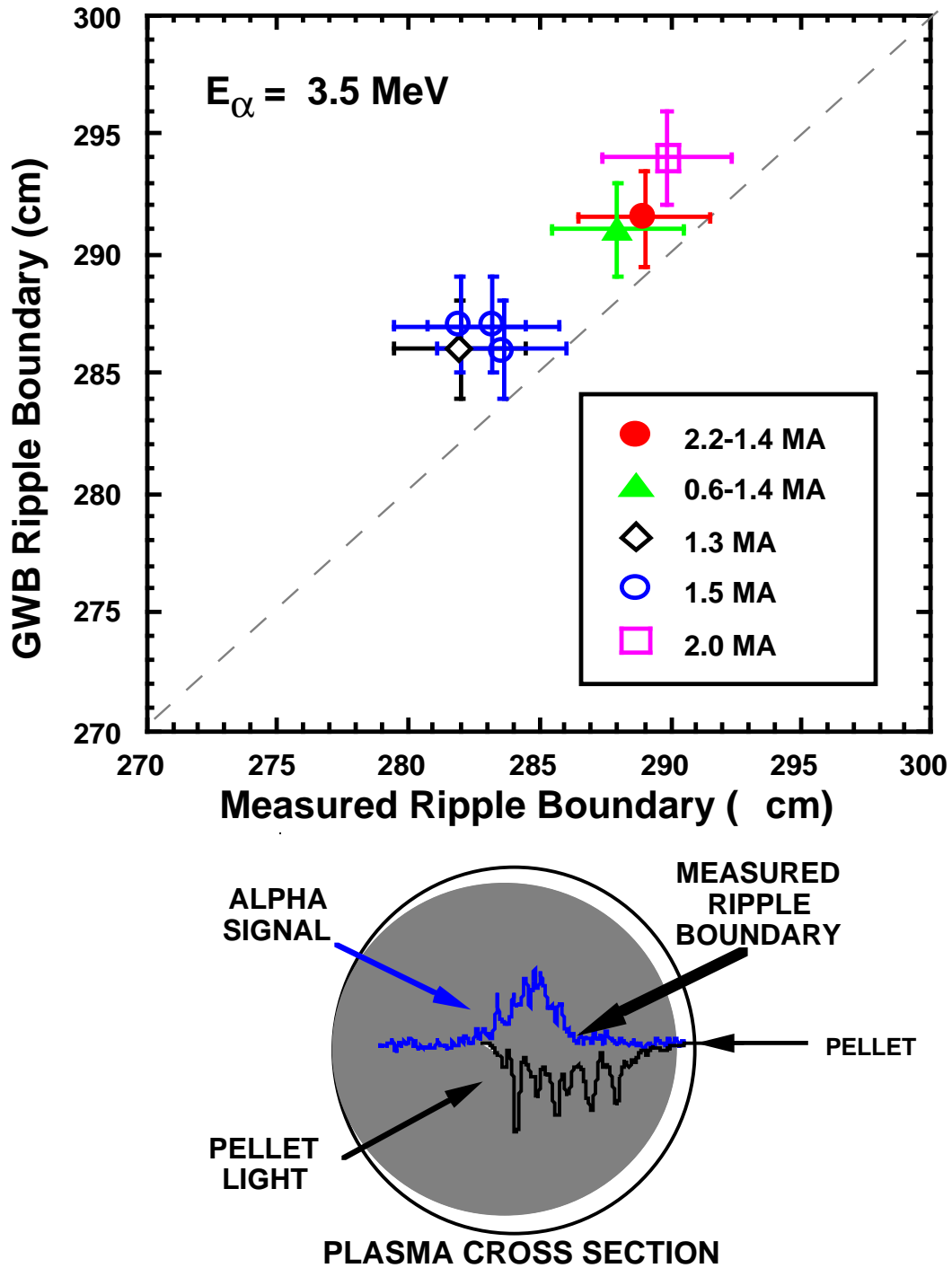


Fig. 24. Comparison of the stochastic ripple boundary from PCX measurements with the Goldston-White-Boozer theory at different plasma currents. The measured ripple boundary corresponds to the major radius at which the PCX alpha signal begins to rise, as illustrated by the insert.

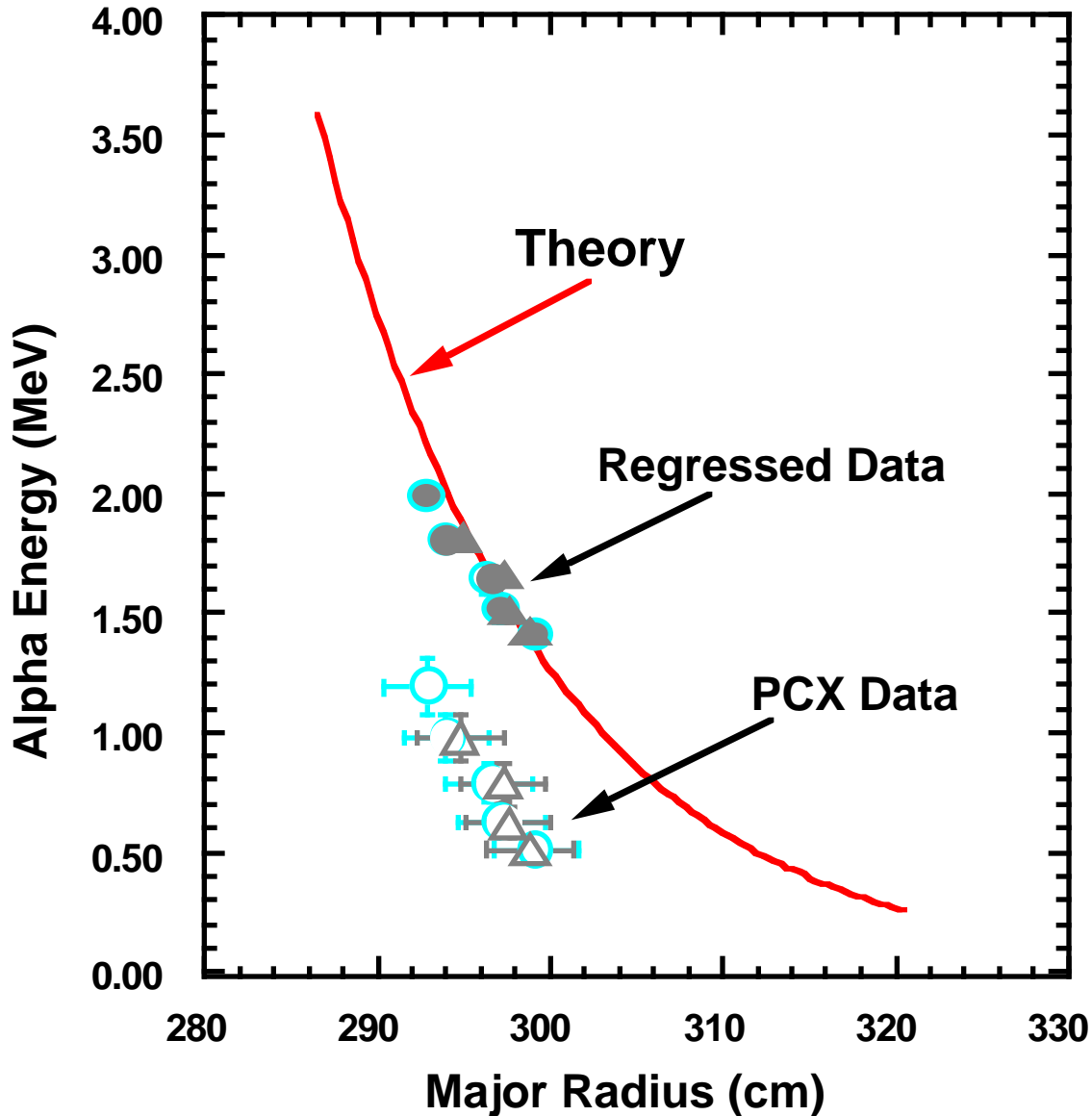


Fig. 25 Measured stochastic ripple boundary as a function alpha energy after sawtooth activity, which redistributes low energy alphas beyond the 3.5 MeV birth alpha boundary. The open data points are the PCX measurements which were taken 120 ms after the sawtooth crash. For the corresponding hatched points, the energy of the measured alpha has been regressed back to the actual time of the sawtooth crash.



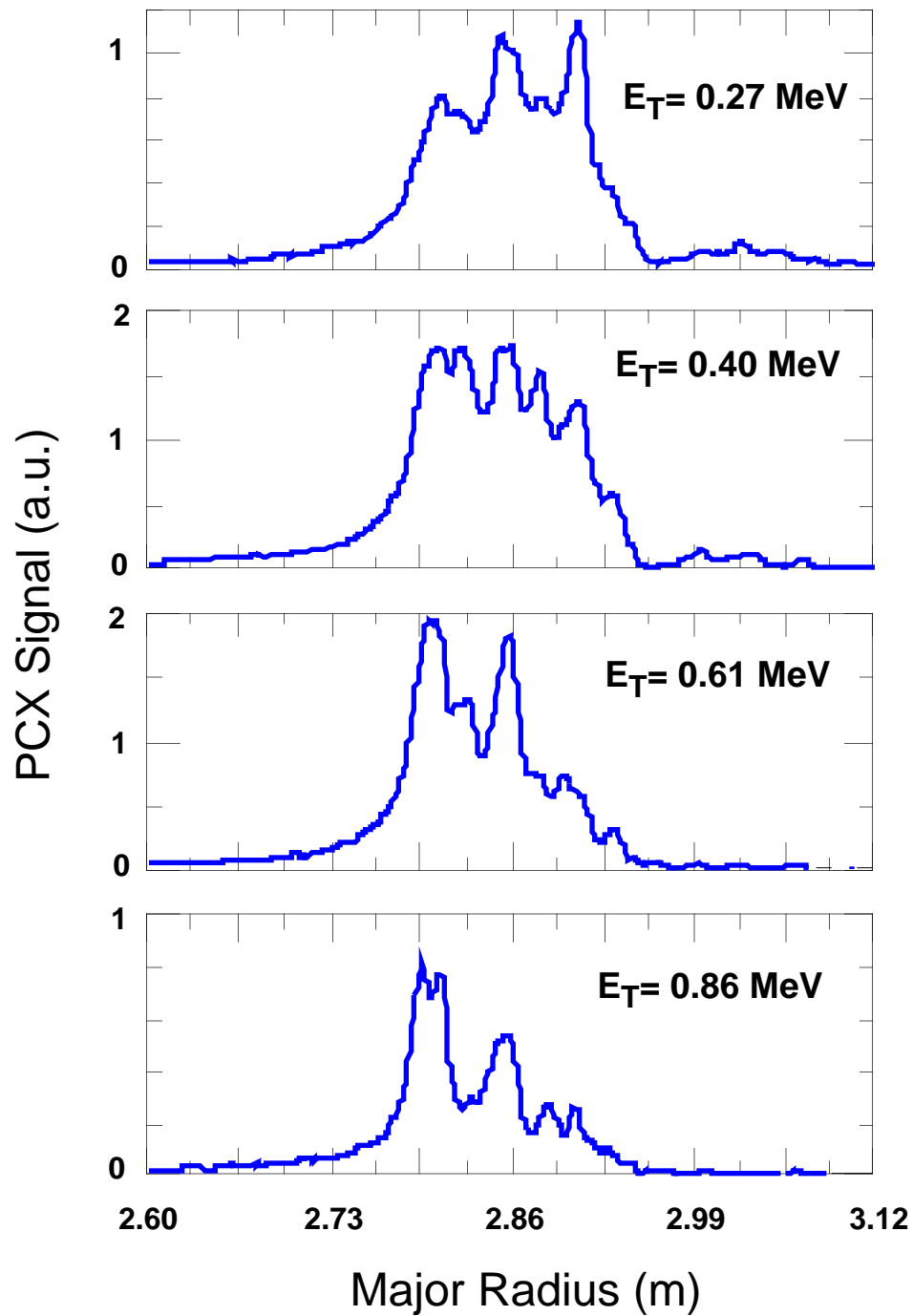


Fig. 26 PCX signals at selected energies for RF-driven tritium ion tail measurements (#89059).

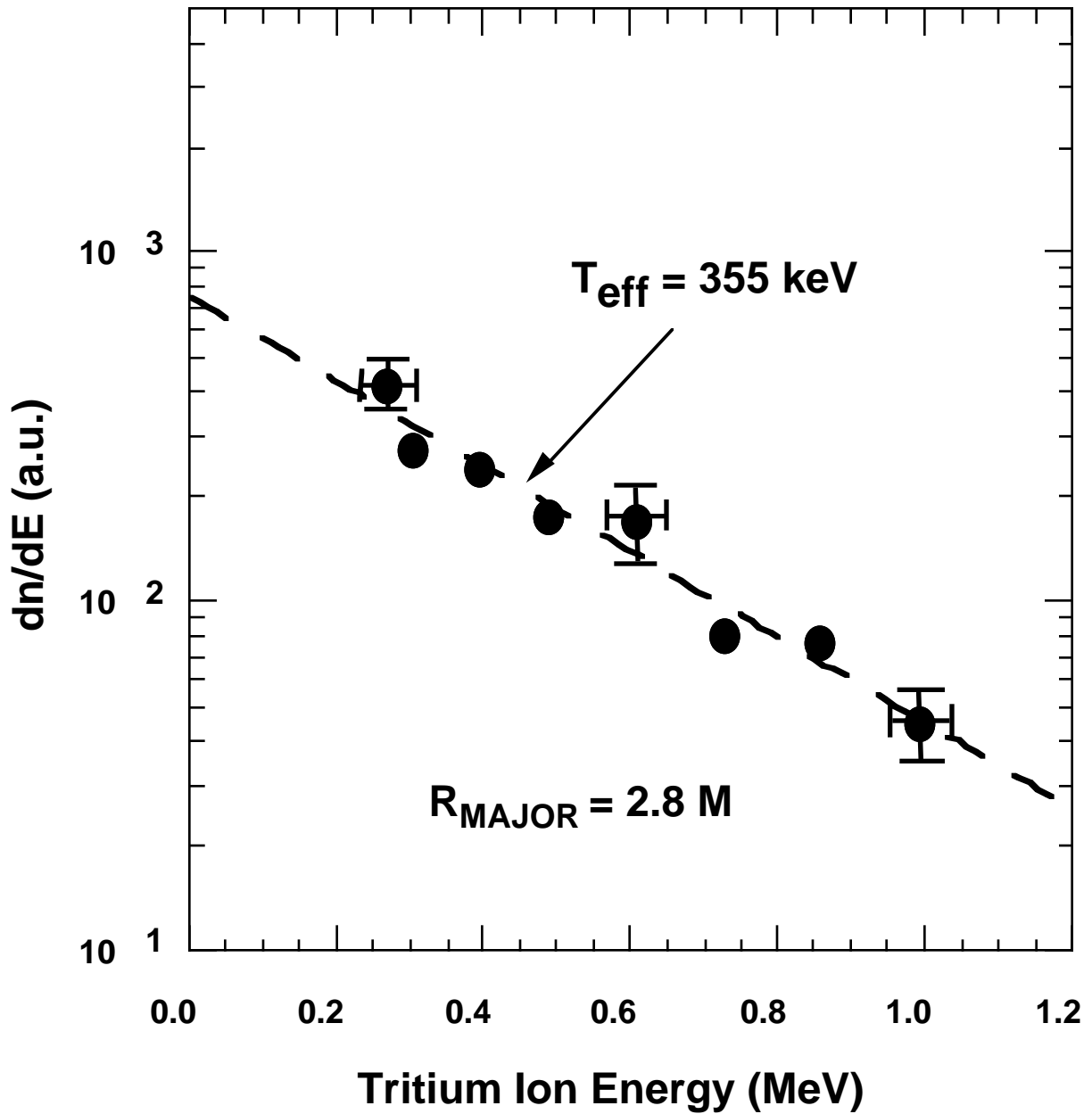


Fig. 27 Tritium tail energy spectrum measured during  $2\Omega_T$  heating. The analysis includes correction for reionization of the exiting tritium neutrals, which increases  $T_{\text{eff}}$  by  $\sim 15\%$  compared to the uncorrected spectra.

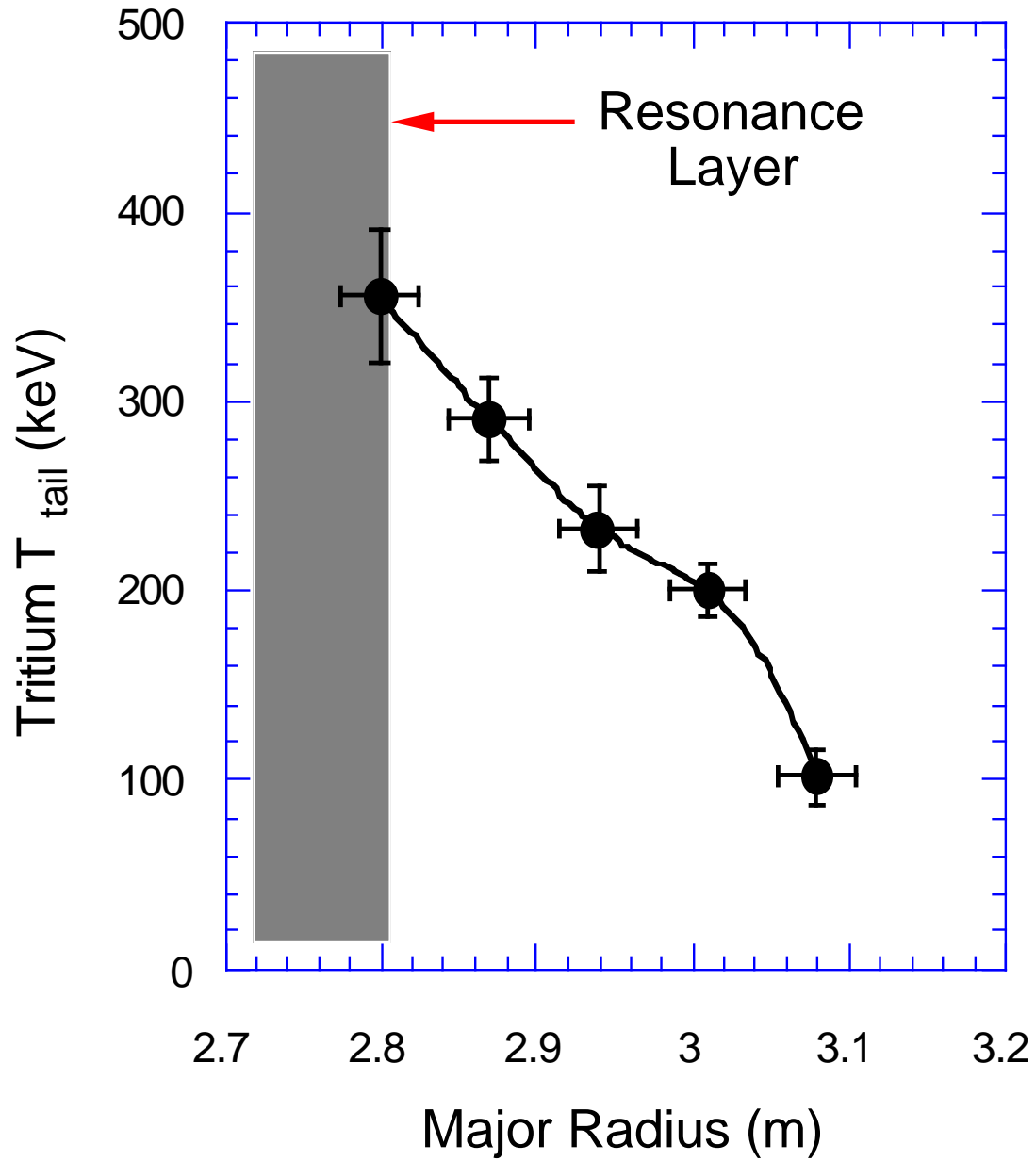


Fig. 28 Radial profile of the effective tail temperature for RF-driven tritium ions measured during  $2\Omega_T$  heating.